POLITECNICO DI MILANO

Facoltà di Ingegneria Industriale

Corso di Laurea Magistrale in Ingegneria Aeronautica

Free-form methodology for aero-structural optimization of wind turbine blades.

Relatore: Prof. Carlo Luigi Bottasso

Co-relatore: Prof. Alessandro Croce

Tesi di Laurea di:

Luca SARTORI Matr. 763764

Anno Accademico 2012 - 2013

Acknowledgements

During the development of this work, I enjoyed the support and the encouragement of several people, and I feel indebted with them. First of all, I want to reward the staff of *PoliWind* research unit at Politecnico di Milano, and especially prof. C. L. Bottasso, prof. A. Croce and F. Gualdoni, for their constant support and their precious advice. On the Dutch shore, I want to express my gratitude to Dr. F. Grasso, who attended the uneasy task of being my supervisor at ECN, and to my colleagues from WET unit, with a special thanks to Ms.O. Ceyhan and Mr. J.M.Peeringa. My gratitude goes also to ECN/NRG interns, together with my best wishes for a bright future. Among the others, I want to acknowledge Prof. André Tits, from the University of Maryland, and Dr. B. Jonkman from NREL. A special thanks goes to Dr. J.P. Blasques, from Risø-DTU Denmark, for the constant and enlightning support for what concerns the functioning of BECAS.

Abstract

The design of wind turbine blades is a multi-disciplinary task, which requires to deal with multiple objectives and constraints, often in conflict with one another. Concerning the aerodynamic design of the blade, current strategies require that the characteristics of airfoils are selected at the beginning of the process, usually under genuine two-dimensional considerentions. Subsequently, the shape and the structural properties of the blade are determined by an optimization process, which allows to maximize the blade performances in a direction which fulfills a set of active constraints. Considering that the initial choice of the airfoils can influence the final design in a substantial manner, this procedure implies some degree of uncertainty. Since the airfoils are considered frozen through the entire design process, this poses relevant limits which prevent a full exploration of the design space. This work investigates an innovative free-form approach for the aero-structural design of rotor blades. This method includes the airofil shapes directly in the optimization process, in order to perform a simultaneous optimization of traditional design variables like chord, twist and structural elements together with the various airfoils along the blade. As a consequence, a higher level of sensitivity is expected, as much as an improved ability to explore the design domain. Since the airfoil shapes are automatically tailored to the evolution of the blade, this should result in a lower influence of the initial choice on the final configuration, leading to better performances of the blade and, eventually, of the entire wind turbine.

Keywords: Wind energy, blade optimization, airfoil design, aero-structural analysis, multi-disciplinary approach.

Riassunto

Intoduzione

L'idea di questo lavoro parte da alcune considerazioni riguardo lo stato dell'arte nell'ottimizzazione di pale eoliche. In particolare, per quanto riguarda il progetto aerodinamico, la pratica corrente consiste nello scegliere un set di profili alari che vengono poi assegnati alla pala. Successivamente, il design globale della pala viene svolto per mezzo di una procedura di ottimizzazione vincolata che consente di ottenere un design ottimo in termini di alcune variabili di progetto, che tipicamente includono corda e twist della pala, così come variabili legate alla struttura della pala. Il fatto che i vari profili non cambino durante l'ottimizzazione, pone dei seri limiti sulla reale efficacia dell'ottimizzazione, in quanto restringe significativamente il dominio di ricerca e costringe il design della pala in una direzione che dipende fortemente dai profili scelti inizialmente.
Questo lavoro si propone di studiare le potenzialità di una metodologia di ottimizzazione *free-form*, in cui le forme dei singoli profili siano lasciate libere di variare, come ogni altra variabile interessata dall'ottimizzazione. Lo scopo del lavoro è lo sviluppo di un algoritmo di ottimizzazione che consenta il design simultaneo di pala (sia aerodinamicamente che dal punto di vista strutturale) e profili. Per lo sviluppo del programma, si è scelto di affidarsi a modelli matematici generalmente semplici, in modo da non mantenere lo sforzo computazionale entro limiti accettabili, ma allo stesso tempo si è posta particolare attenzione nel rispettare, seppur in forma semplificata, i vincoli progettuali che determinano normalmente il design della pala. I risultati attesi sono:

- Una maggiore sensibilità della procedura di ottimizzazione che, potendo adattare liberamente i profili al resto della pala dovrebbe garantire migliori performance della soluzione finale.
- Una minor responsabilità del designer nella scelta dei profili iniziali.

Metodologia

per la risoluzione numerica del problema di ottimizzazione, questo lavoro impiega un solutore di tipo SQP (Sequential Quadratic Programming) basato su un

metodo a gradiente. Il design evolve in modo da massimizzare in modo iterativo una certa cifra di merito, sotto l'azione di vincoli imposti dall'utente. In particolare, come molti lavori nel campo dell'energia eolica, la cifra di merito adottata è il costo dell'energia, che rappresenta la grandezza migliore da minimizzare, in quanto è capace di tenre in considerazione tutti i diversi aspetti della vita operativa della macchina. I vincoli che vengono imposti affinché la soluzione rimanga fisicamente accettabile, riguardano essenzialmente la struttura della pala, in particolare:

- La prima frequenza di flappeggio dev'essere maggiore della frequenza naturale 3P (comunemente chiamata tre-per-giro).

- Lo sforzo nei singoli elementi strutturali deve mantenersi inferiore a un valore massimo ammissibile.

E' importante notare che tali vincoli, per quanto generali, sono in grado di riprodurre vincoli progettuali realmente applicati nel design di pale eoliche di notevoli dimensioni.
Per quanto riguarda la simulazione della pala, l'algoritmo è diviso in tre sottoproblemi principali, ognuno dei quali agisce su un aspetto fondamentale del design globale:

- **Analisi aerodinamica 2D**. La stima delle proprietà aerodinamiche dei vari profili dev'essere svolta ad ogni iterata. All'interno del programma, ogni profilo lungo la pala viene prima generato attraverso curve di tipo Bézier, e poi analizzato con `XFOIL` in modo da ottenere dati sulla portanza, resistenza e sul momento in un range di angoli $\pm 20^{circ}$. Tali dati vengono poi estesi all'intero range $\pm 180^{circ}$ mediante il modello di estrapolazione di Viterna-Corrigan.

- **Analisi aerodinamica 3D**. Il comportamento aerodinamico della pala è calcolato mediante la teoria dell'elemento di pala (BEM) unita a una distribuzione delle proprietà dei profili ottenute al punto precedente. Il modello di vento è molto semplice, stazionario e uniforme, e l'output principale di questa simulazione è l'energia prodotta annualmente (AEP).

- **Analisi strutturale**. Da un punto di vista strutturale, la pala è rappresentata con un modello di pala 1D associato a proprietà di massa e rigidezza in un numero arbitrario di sezioni. Queste ultime sono ottenute mediante analisi a Elementi Finiti superficiali, che viene svolta su ogni sezione in esame. In questo modo, anche gli sforzi locali nei vari elementi vengono verificati. Attraverso il modello 1D, a sua volta discretizzato in Elementi Finiti, è possibile calcolare le frequenze della pala e assicurare il soddisfacimento anche del vincolo sulla frequenza.

Il calcolo della cifra di merito viene poi svolto prendendo come input l'energia prodotta e il peso della pala, che determinano sostanzialmente il costo finale dell'energia. Il modello di costo adottato è molto raffinato e permette di considerare non solo i costi direttamente legati alla pala, ma anche all'intero impianto.

Risultati

L'algoritmo per la metodologia free-form è stato testato pale di diverse dimensioni. In questo lavoro vengono proposti due casi, entrambi basati su macchine reali e progettate con criteri di ottimizzazione tradizionali. La prima pala è una tipica macchina da 2MW, caratterizzata da una pala di 45 metri, a cui sono stati assegnati cinque diversi profili 'attivi', cioè integrati nell'ottimizzazione. Il secondo caso è una pala da 10MW, progettata presso la Technical University of Denmark e adottata come reference nel contesto del consorzio INNWIND. In entrambi i casi, i risultati dimostrano una buona capacità dell'ottimizzatore di gestire il design della pala, in particolare per quel che riguarda lo sviluppo dei profili, oggetto di questa tesi. E' interessante notare come profili sistemati in zone diverse della pala subiscano percorsi di ottimizzazione diversi, e si riscontra una certa coerenza con la realtà progettuale e manifatturiera delle pale eoliche. in particolare, profili posti vicino alla radice della pala tendono a ridurre il proprio spessore, per ridurre il peso, ma al contempo ad aumentare lo spessore al bordo di uscita (diventando cioè profili flatback). Ciò viene fatto autonomamente dall'ottimizzatore, in modo da compensare la perdita di rigidezza flessionale causata dalla riduzione di spessore. Profili cosiddetti mid-span, ovvero nel mezzo della pala, presentano invece un design che favorisce l'aerodinamica. in genere, presentano uno spessore simile ai profili di partenza ma una curvatura decisamente superiore, in modo da produrre più portanza e migliorare l'efficienza. Si nota anche come l'introduzione di carichi superiori venga generalmente compensata dall'ottimizzatore attraverso altre variabili. profili di estremità, invece, presentano generalmente una geomteria intermedia, con uno spessore molto ridotto rispetto a quelli iniziale e una curvatura aumentata di poco, in modo da non introdurre carichi troppo alti che andrebbero a contribuire significamente al momento flettente in radice. Interessante notare anche come il design della prima pala (2MW) sia dominato dal vincolo di frequenza, mentre il desing della seconda pala è dominato da considerazioni di sforzo.

Conclusioni e Sviluppi Futuri

Alla luce delle prove svolte, è possibile affermare che l'obiettivo della tesi è stato raggiunto. In particolar modo, è incoraggiante il fatto che l'ottimizzatore sia in grado di operare dei miglioramenti anche quando la pala di partenza presenta

già un design molto buono. Un'altro punto soddisfacente riguarda la capacità dell'algoritmo di gestire una gran quantità di variabili di progetto, molto diverse tra loro, in modo coerente de efficace. Specialmente per quello che riguarda i profili, è interessante vedere come vincoli di natura molto generale abbiano in realtà effetti locali motlo importante sul design del singolo profilo.
Dal momento che lo scopo di questa tesi è uno studio preliminare, si propongono alcuni spunti per eventuali studi futuri. In particolar modo:

- Sostituire `XFOIL` con un solutore numerico più accurato, in modo da avere una migliore risoluzione della regione di stallo
- Migliorare l'accuratezza della parte strutturale, in particolare attraverso un miglior dettaglio nella descrizione della sezione di pala. Futuri sviluppi del codice dovrebbero permettere il dimensionamento di tutti gli elementi principali della struttura.
- Testare il codice con modelli più accurati, in modo da verificarne il comportamento anche di fronte a vincoli di buckling, o di fatica.

Contents

List of Figures

List of Tables

Chapter 1

Introduction

In the last years the harvesting of wind power for energy production has increased dramatically, leading to a significant interest in the development of methodologies for the design of the new generation of wind turbines. In this context, the numerical optimization techniques can provide a valuable support in the design process, and at present they are largely employed both in the industry and within research institution. Since modern wind turbines are charactherized by large rotor sizes and by a power production in the range of several megawatts, the optimization of a rotor blade is a complex problem, which must be addressed with a strong multi-disciplinary approach. A variety of physical phenomena affect the final design, and several considerations should be made in order to drive the optimization towards an optimal solutions which can improve the behavior of the blade. At the same time, a set of constraints should be imposed, in order to maintain the design within the tracks of a phisically-meaningful solution. As a result, after optimization a rotor blade must represent the best compromise between conflicting requirements, which involve aerodynamic performances, structural efficiency and dynamic response as much as considerations about convenience and economic feasibility of the project.

1.1 Scope and methodology of this work

The determination of the aerodynamic behaviour of the blade is an essential step during the design of a new wind turbine. In the most known algorithms for wind turbines optimization, the aerodynamic loads are generally computed by a three-dimensional model, like BEM methods or the lifting line theory, coupled with a span-wise distribution of the airfoil aerodynamic characteristics, typically the lift and drag coefficients and the pitching moment. Then, the full aero-structural optimization of the blade can be summarized in the following procedure:

- At the beginning of the process, the various airfoils along the blade are chosen. The airfoils can be selected from existing families or new airfoils can

be designed on purpose, in order to meet the local requirements. Usually, the choice is driven by both aerodynamic and structural considerations.

- A blade optimization is performed, with the required level of detail:
  - The chord, twist and other relevant properties like precone angle and sweep are determined, in order to maximize the annual energy production.
  - The various structural elements are sized under dynamic and aeroelastic considerations, which typically include fatigue, ultimate loads and buckling in order to comply with international standards.
- The final blade is tested with high-complexity models, which include all the operating conditions and the load envelopes, in order to identify and correct possible weakspots which persist after optimization.

Although this strategy is well-established in wind turbines design, it implies some relevant limitations. In fact, as long as BEM or lifting line models are employed, the overall aerodynamic behaviour of the blade is estimated starting from the local two-dimensional properties of the airfoils. This means that the initial choice of the airfoils can affect the optimization in a significant way, basically because it poses a serious restriction on the feasibility domain in which a solution is researched. The drawback is that usually the resulting blade is only a sub-optimal solution of the optimization process.

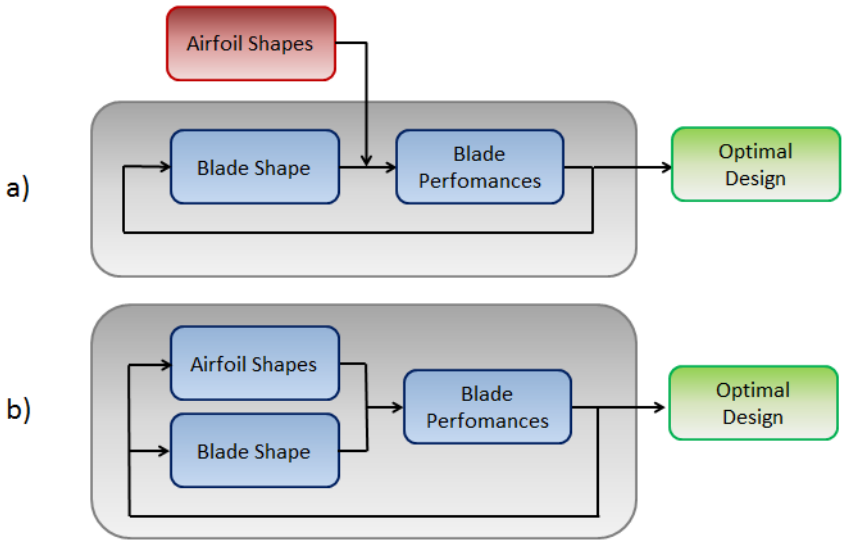

Figure 1.1: Comparison between a) a traditional blade optimization approach and b) the *free-form* approach

This work explores an integrated *Free-Form* methodology for the aero-structural optimization of rotor blades. The fundamental idea is to include the airfoil shapes directly within the optimization process, so that the local aerodynamic performances can be adjusted in order to comply with the evolution of the blade design. Under a practical point of view, this means that the shapes of the airfoils along the blade are no longer considered frozen, but they are left free to change during the analysis, like any other design variable involved in the optimization.
Figure 1.1 shows a comparison between the workflow of a traditional optimization algorithm and the free-form methodology investigated in this work. The main advantage of the free-form approach is that the optimization can affect directly the airfoil shapes, which are no longer treated like a forcing term. This should assure that the optimization is done with a higher level of sensitivity, thus granting a full exploitation of the domain of feasibility and, consequently, better performances of the final wind turbine. From a practical point of view, the fact that the airfoils are constantly modified during the analysis should decrease the importance of their initial choice, thus relieving the designers from a delicate *a priori* choice.

In the following, we illustrate the development of a numerical algorithm for the free-form optimization of rotor blades, which main goals are:

- to explore the feasibility of this methodology, that is, to verify if standard numerical optimization techniques can be used to handle the extended set of the design variables without bad-scaling or ill-conditioning problems.

- to test its convenience against the traditional strategies illustrated above. Presumably, the greater level of freedom experienced by the optimization should lead to an improved design, even if the starting point is represented by a high-efficiency initial blade.

The algorithm illustrated in this work is conceived to deal with optimization of large to very-large wind turbines, which means that the strong interaction of different phenomena requires to follow a multi-disciplinary approach. We must consider that the evolution of the airfoils brings severe implications on both the global aerodynamic behaviour of the blade, because of the local variation in lift, drag and efficiency, and the structural design, since a variation of the airfoil thickness affects the sectional area, and thus the local stiffness and mass matrix. For this reason, the program for the free-form methodology supports a variety of analysis, which allow to take into consideration not only the aerodynamic issues related to the design of the airfoils, but also their implications on structural sizing and on dynamic response.
Figure 1.2 shows the logical flow chart of the algorithm, which puts in evidence the three essential sub-problems of the blade optimization, specifically the design of the airfoil, the aerodynamic and the structural optimization of the blade. The

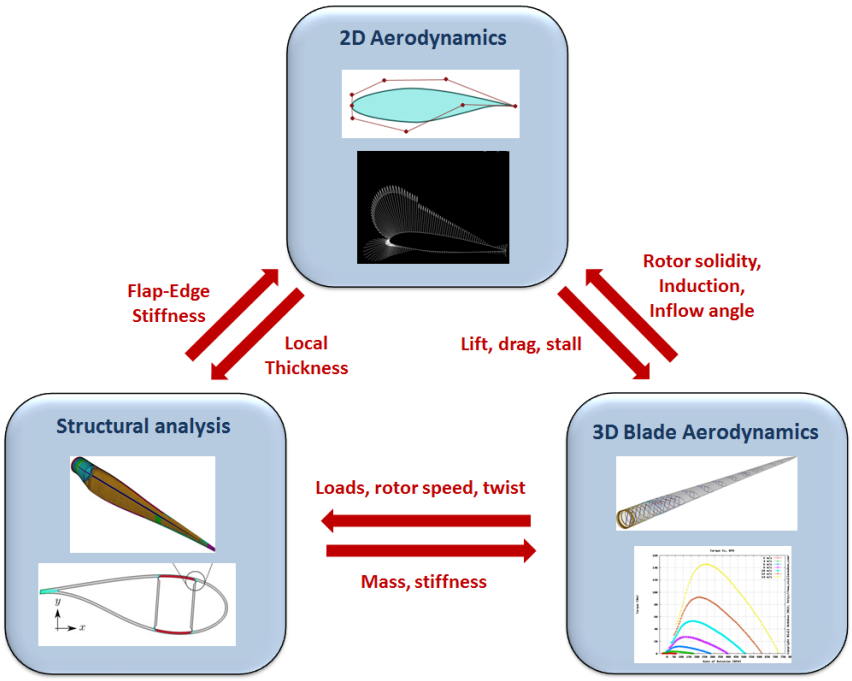

Figure 1.2: Integrated aero-structural approach.

red arrows highlight the mutual interferences between the different aspects of the design, which are actually related to one another. The realization of the algorithm is driven by two, partially conflicting, ideas:

- Simplicity. Since the goal of this work is to investigate a new methodology, the algorithm is not expected to offer a high level of complexity. Rather, it is based on popular and well-validated models which are typically employed in the optimization of rotor blades at a preliminary level.

- Completeness. Although its intrinsic simplicity, the program offers all the necessary capabilities required by standard international guidelines for wind turbine design.

Since the program is conceived to be used by anyone with confidence, a great care is taken in order to optimize the computational effort required by the algorithm. As a result, and regerdless to the practical outcomes of this work, a secondary result is that the new algorithm represents a good point of compromise between accuracy and simplicity, and it could be used for preliminary optimization of new rotor blades in spite of commercial, high-complexity codes.

1.2 State of Art

The use of numerical optimization in wind turbines design has been extensively investigated in the literature. However, although a great research effort, there are still few examples of dedicated algortihms for the systematic solution of the optimization problem. Here, a quick survey of the most relevant softwares is proposed, in order to cast light on the role of this work in the framework of the available material.

1.2.1 Blade Optimization Tool

This program, which was developed at the Energy Research Centre of the Netherlands, is able to maximize the annual energy production of a rotor blade by optimization of traditional shape parameters of the blade, specifically the chord and the twist [1] distribution. At the beginning of the analysis the user is required to provide an intial blade shape, together with aerodynamic data for the different airfoils along the blade. Then, the stationary aerodynamic performances of the blade are estimated by means of the blade element momentum (BEM) theory, and a gradient-based method manages the evolution of the chord and twist design until an optimal solution is found. The program is distributed as an Excel workbook, and shows a very intuitive grafic interface, which is illustrated in Figure 1.3.

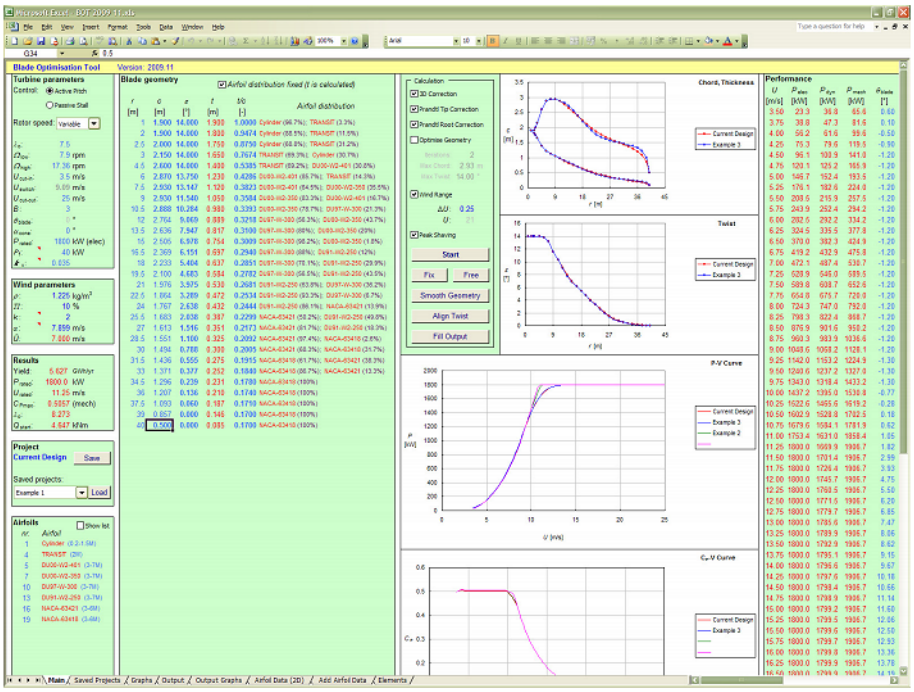

Figure 1.3: User interface of the Blade Optimization Tool

In order to make the computation of the AEP more accurate, within the BOT environment the user has several option in order to personalize the analysis. In particular, several corrections can be implemented in the BEM solver in order to refine the accuracy, like tip-losses and hub-losses models which can account for typical three-dimensional phenomena with an acceptable degree of fidelity. The user can also set a maximum chord and a maximum twist in order to bound the optimization process, and can require to smooth the optimal blade in order to make it suitable for manifacture. The essential limitation of this tool is that a structural model of the blade is absent, and this requires that the structural design of the blade is carried-out separately. Unfortuntely, since the cross-effects between the aerodynamic and the structural aspects of the design are actually strong, this limitation could have several implications in the overall design capabilities of this software.

1.2.2 Harp_Opt

The HARP_Opt (Horizontal Axis Rotor Performance Optimization) is an example of a more integrated optimization tool. It was developed at the National Renewable Energy Laboratories (NREL) and it is basically open-source, since it uses several free-solvers developed by NREL in the last years. HARP_Opt exploits the Matlab genetic algorithm library to design horizontal-axis wind and hydrokinetic turbine rotors, working on both the aerodynamics and the structural aspects of the design. Specifically, the aerodyamic design is driven by maximization of the AEP, and the procedure for its estimation is similar to that of BOT: first, a traditional BEM model is used for the estimation of the power curve. Then, the Weibull or Rayleigh distributions are used in order to adapt the power curve to a specific wind site. For the structural analysis, the blade is modeled as a thin shell of bulk isotropic material, and the blade mass is minimized using a maximum allowable strain as constraint. In particular, the strain is evaluated at four different points on each section, as illustrated in Figure 1.4. This allows to control the thickness of the shell, in order to maintain the strain under a fixed allowable value.

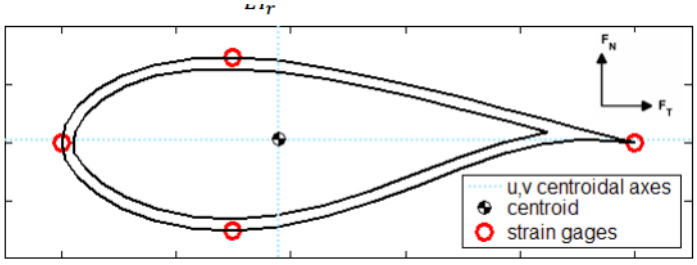

Figure 1.4: Strain-detection gauges on a typical HARP_Opt section.

Although this program can somewhat consider the structure, there are still rele-

vant limitations. First, the two problems (aerodynamic and structural) are not merged in a single integrated optimization process, but they are still considered as two independent sub-problems. Second, since only the shell is modelled, the description of each section is quite elementary, and allows only a verification of the structural properties rather than an organized and focused design.

1.2.3 Cp-Max

The *PoliWind* research unit at Politecnico di Milano spent a significant effort on the development of numerical tools for the multi-disciplinary optimization of wind turbines, and the result is the Code for Perfomance Maximization (Cp-Max) [2]. The program provides a set of routines for the aero-servo-elastic analysis and design of the entire wind turbine, and the capabilities of the solver include aerodynamic loads estimation, implementation of control laws, dynamic and aero-elastic simulations and sizing of various structural elements.

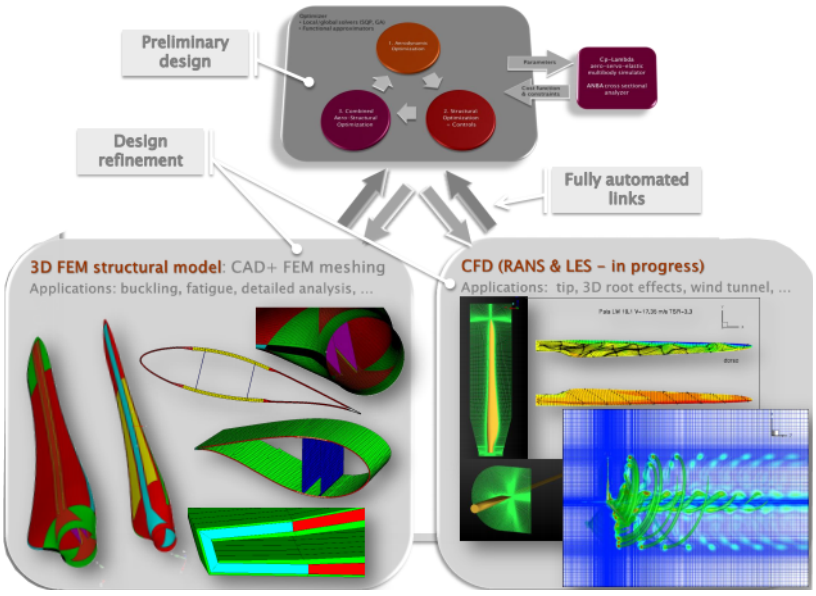

Figure 1.5: Architecture of Cp-Max.

The program allows to minimize the cost of energy under a set of constraints which are imposed by the user. The functioning, that is, the research of an optimal solution is based on two subsequential steps: at first, the program operates a global optimization of an intial blade, where some global parameters are fixed, like for example the radius or the maximum chord. After that, the analysis is repeated for a number of different global parameters, until a family of optimized blades is generated. Subsequently, the various optimal solutions are interpolated in order to identify the actual optimal solution, which can be analyzed with high complexity models in order to assure that it fulfills all the constraints. A sketch

of the architecture of the program is provided in Figure 1.5. The advantage of Cp-Max is that it offers a high level of detail in the simulation of the wind turbine from the very preliminary stages of design but, on the other hand, it still relies on combined 2D/3D models for the aerodynamic analysis of the blade, that is, the user must still provide data about the various airfoils.

1.3 Considerations about the state of art

The available resources employed for rotor blade optimization offer a variety of methodologies and different levels of detail. It is reamrakble to notice that at present the need for complete aero-structural models is largely accepted but, however, the idea of including the airfoils within the optimiztion process seems to remain unexplored. In this context, this study can offer a stronger insight of what concerns the capabilities of modern optimization techniques, particularly about the strategies which drive the design of wind turbines-dedicated airfoils. As traditional optimization techniques are somewhat limited by the need to provide airfoils data, the algorithm for the free-form approach can offer a more flexible tool and could represent a significant step towards a truly integrated blade design. From a practical point of view, this program can represent also a reliable, though simple, start point for further more accurate investigations.

This work, and specifically the algorithm, has been developed within a joint-project between Politecnico di Milano and the Energy Research Centre of the Netherlands (ECN), and is partially supported by the FP7 INNWIND project.

Chapter 2

General Algorithm Description

This Chapter illustrates the high-level features of the free-form algorithm developed in this work. The scope is to illustrate how the algorithm can address and manage the optimization of large rotor blades and to identify, among different strategies, which best suit the needs of this study. First, the formulation of the general optimization problem is provided, together with a brief account of the available techniques for its numerical solution. The features of the gradient-based SQP methods are also revised, in order to explain which considerations make these methods a good choice. It follows a description about the need to solve the aero-structural blade design problem with a multi-disciplinary approach and, in particular, the choice of the objective function and constraints is discussed extensively, as they play a crucial role in the behaviour of the optimization algorithm.

2.1 The Optimization Problem

Optimization is an iterative procedure which is able to find the point of minimum of a multi-dimensional function while granting, at the same time, that a set of active constraints is respected at each iteration. Under a mathematical point of view, a traditional optimization algorithm can be expressed by the problem:

$$find: \ \ min\{f(\boldsymbol{x})\} \tag{2.1}$$

so that:

$$\begin{aligned} bl_i \leq x_i \leq bu_i \\ g_j(\boldsymbol{x}) \leq 0 \ \ j = 1, ..., n_i \\ h_j(\boldsymbol{x}) = 0 \ j = 1, ..., n_e \end{aligned} \tag{2.2}$$

where $\boldsymbol{x} = \{x_1, x_2, ..x_n\}$ is the set of the design variables, $f(\boldsymbol{x})$ is the objective function. bl_i and bu_i represent the boundary values for each design variable x_i

and define the searchable design space, while g_j and h_j are, respectively, a set of inequality constraints and a set of equality constraints for the problem. The constraints divide the design space into two domains, the feasible domain, where the constraints are satisfied, and the infeasible domain where at least one of the constraints is violated. In most practical problems the minimum is found on the boundary between the feasible and infeasible domains, that is at a point where $g_j(x) = 0$ for at least one j . In many aerodynamics and wind energy applications, the use of inequality constraints is of paramount importance, as the unconstrained optimization can evolve towards an unphysical configuration: for a detailed example, the reader can refer to [3]. In the general case, the objective and constraint functions can be linear or non-linear and can be explicit or implicit functions. This is the case, for example, when numerical techniques are employed to evaluate the objective function or the constraints, as in the Finite Elements Methods. Although the problem (2.1) is expressed by analitical functions, in the majority of applications the design variables are not required to be continuous, but they are provided in some discrete form.

2.1.1 Sequential Quadratic Programming

The problem of finding a solution of the (2.1) under the set of constrains imposed by the (2.2) has been extensively studied in the past, and represents a primary research topic in the field of the applied mathemathics. The increasing efficiency of the numerical optimization techniques ensures that high-complexity problems can be addressed in a variety of engineering fields. At present, several techniques are available for the numerical implementation of the optimization problem, and an interesting review of them is provided in [4], where the fundamental differences between local optimization and global optimization algorithms are illustrated and discussed. In order to identify which techniques best suits our scopes, it must be kept in mind that this work shows some peculiarities which can heavily affect the optimization process. Specifically:

- Since a set of airfoils-related variables is added to the traditional set of the design variables, we expect that the optimization should manage a large amount of parameters.
- In order to represent phisical phenomena which limit the design, we need to provide a set of nonlinear constraints, in order to bound the research domain.
- A reasonable computational time (hours/days)is also a requirement, especially at the early development stage, when bugs and errors must be detected and fixed as soon as possible.

These considerations led to the choice of a gradient-based method, which typically assures good convergence properties and a good handling of the inequality

constraints. Specifically, for what concerns the optimization process, our algorithm relies on an open-source Sequential Quadratic Programming algorithm [5]. This module was developed at the University of Maryland and it has been tested in several applications. Mathematically, an SQP models the non-linear problem with a Quadratic Programming (QP) subproblem, which is solved for the iterate $\boldsymbol{x}_k$. The solution of the QP subproblem is then used to generate the iterate $\boldsymbol{x}_{k+1}$. Recalling the problem (2.1) and the constraints (2.2), the *feasibility region* is defined as the set of points satisfying:

$$F \equiv \{\boldsymbol{x} \in R^n \mid h(\boldsymbol{x}) = 0,\ g(\boldsymbol{x}) \leq 0\} \tag{2.3}$$

The Lagrangian functional associated with the non-linear problem is:

$$\mathcal{L}(\boldsymbol{x}, \lambda, \mu) \equiv f(\boldsymbol{x}) + \lambda^T h(\boldsymbol{x}) + \mu^T g(\boldsymbol{x}) \tag{2.4}$$

The QP subproblem for the objective function is built by replacing f by its local quadratic approximation:

$$f(\boldsymbol{x}) \simeq f(\boldsymbol{x}_k) + \nabla f(\boldsymbol{x}_k)(\boldsymbol{x} - \boldsymbol{x}_k) + \frac{1}{2}(\boldsymbol{x} - \boldsymbol{x}_k) H f(\boldsymbol{x}_k)(\boldsymbol{x} - \boldsymbol{x}_k) \tag{2.5}$$

where H is the Hessian of f. The QP subproblems for the constraints are obtained by replacing g, h with their affine approximations:

$$\begin{aligned} g(\boldsymbol{x}) &\simeq g(\boldsymbol{x}_k) + \nabla g(\boldsymbol{x}_k)(\boldsymbol{x} - \boldsymbol{x}_k) \\ h(\boldsymbol{x}) &\simeq h(\boldsymbol{x}_k) + \nabla h(\boldsymbol{x}_k)(\boldsymbol{x} - \boldsymbol{x}_k) \end{aligned} \tag{2.6}$$

After defining $d(\boldsymbol{x}) = \boldsymbol{x} - \boldsymbol{x}_k$ and $B_k = H f(\boldsymbol{x}_k)$ this leads to the re-formulation of the optimization problem as follows:

$$\begin{aligned} &\textit{minimize}: && \nabla f(\boldsymbol{x}_k)^T d(\boldsymbol{x}) + \frac{1}{2} d(\boldsymbol{x})^T B_k d(\boldsymbol{x}_k) \\ &\textit{over}: && d(\boldsymbol{x}) \in R^n \\ &\textit{so that}: && h(\boldsymbol{x}_k) + \nabla h(\boldsymbol{x}_k)^T d(\boldsymbol{x}_k) = 0 \\ & && g(\boldsymbol{x}_k) + \nabla g(\boldsymbol{x}_k)^T d(\boldsymbol{x}_k) \leq 0 \end{aligned} \tag{2.7}$$

An SQP method can have very good theoretical local convergence properties: quadratic, superlinear or two-step superlinear convergence of the process can be achieved by requiring B_k to approximate $H\mathcal{L}$ in an appropriate manner [6]. Another additional property of the method should be pointed out: SQP is not a feasible-point method, that is, neither the initial point nor any of the subsequent iterates need to be feasible. This is a major advantage, since finding a feasible point inside non-linear constrained problems may be nearly as hard as solving the problem itself.

2.1.2 Modified-SQP for reduction of the computational time

One of the main issues when working with gradient-descent methods like an SQP solver, is the great computational time required by the computation of the gradient. When n degrees of freedom are chosen, the solver needs to compute each derivative $\frac{\partial f}{\partial x_n}$ of the objective function in order to establish the better descent direction. When one or more constraints g_j are imposed, the computation of the gradient is repeated for each constraint in a sequential way, that is, *first* the gradient of the objective function is computed and *then* the gradient of each constraint is calculated. When a great number of design variables is adopted and n approaches 100 or more, this could lead to an outstanding time needed for each single iterate. To avoid this, the standard routines of the SQP solver were modified in order to allow the simultaneous computation of all the derivatives. This is explained in Figure 2.1, which represent a case where two constraints and the objective function are evaluated.

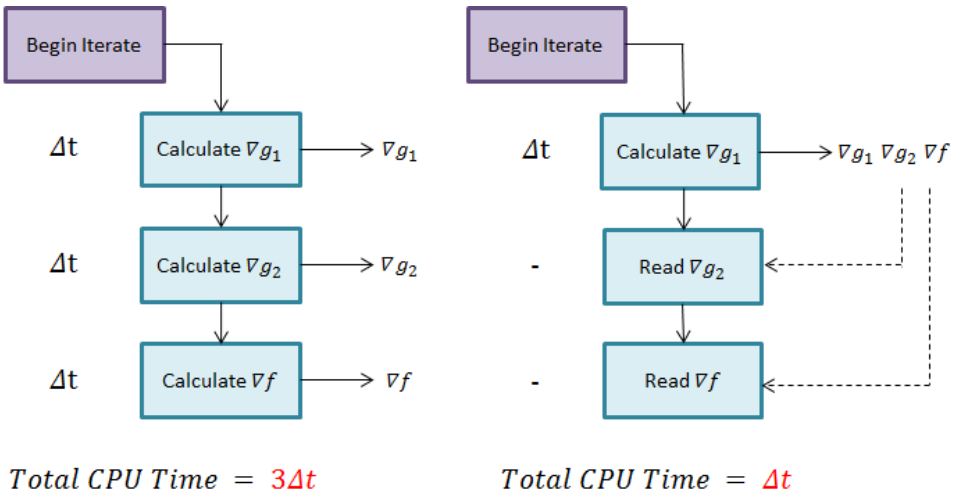

Figure 2.1: Modified SQP for simultaneous gradient computation.

This way, instead of computing each gradient from scratch, all the derivatives are evaluated at the same time when the gradient routine is first invoked. On the subsequent calls of the routine, the program just reads back the values which were computed and saved during the first call. This means that only a third of the time is required for gradient computation, thus saving hours of computational time.

2.2 A multi-disciplinary approach

As mentioned in the introduction, the analysis and design of a modern wind turbine should be addressed with a multi-disciplinary approach. In fact, several

factors influence the overall performances of the machine, and they include aerodynamic performance of the blade, loads computation, control laws implementation and tuning, structural sizing, static and dynamic response. The mutual interferences between these aspects, as long as the presence of several constraints acting on the design makes this kind of analysis a challenging and complex engineering problem. In this work, the formulation of control problems is not covered, as we mainly focus about the analysis and the design of the blade, which must be based upon both aerodynamic and structural considerations. Although we chose to rely on simple and well-validated models for what concerns the blade analysis, a significant care was taken in order to catch all the essential considerations which drive the design of a modern rotor blade. From a practical point of view, the workflow of the algorithm can be subdivided in various sub-problems. Figure 2.2 shows the structure of the program and the main sub-problems which constitute the process. Starting from an intial guess, the optimization algorithm iterates cyclically between the blocks until an optimal solution is found to satisfy the set of the constraints. For each sub-problem, the white window lists all the design variables which are related to it, as much as its specifc contribution to the objective function. Green windows show the constraints which are imposed at each level, while the orange window identifies the objective function.

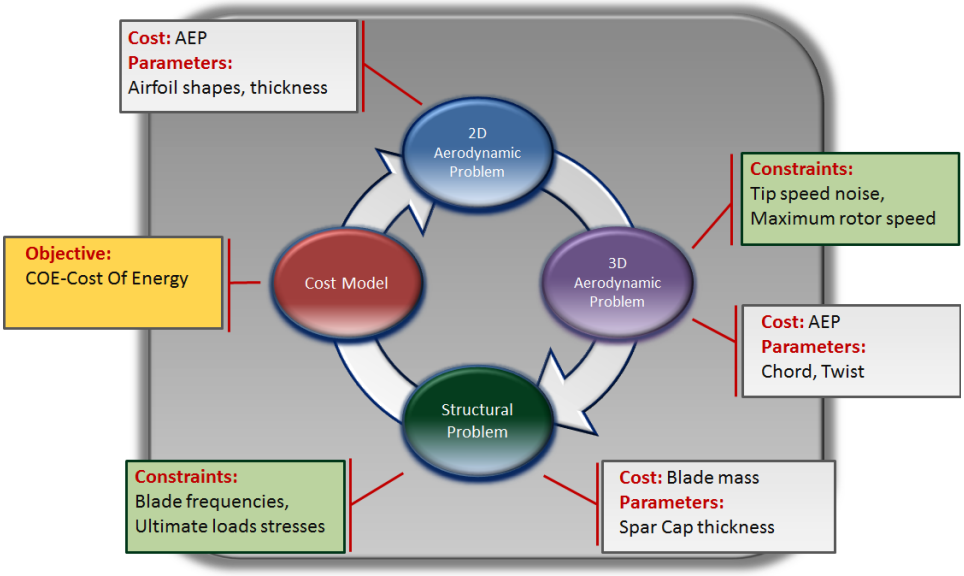

Figure 2.2: Multi-disciplinary approach and design drivers.

The flow-chart of Figure 2.2 is a high-level scheme. Intuitively, each of the sub-problems can be modelled to different levels of detail, without changing the nature of the algorithm. This means that future developments of the algorithm could act on the single models with no need to reshape the entire logical functioning of the program.

Objective function

In wind energy optimization, usually the *Cost Of Energy, COE* is taken as objective function. This is done because, in a global and competitive energy market, the main goal of the wind energy industry is to maintain the costs comparable against traditional energy sources. The Cost Model proposed in [7] was developed by the National Renewable Energy Laboratories, NREL. It is based on a scaling model applied to a traditional upwind, three-bladed wind turbine and allows to link the COE to a series of parameters which include rotor radius, blade weight and Annual Energy Production. These can be easily related to traditional design variables used in the optimization, thus obtaining a single and precise objective function which is capable of taking into account all the aspects of a multi-disciplinary approach. The most common deifinition of the cost of energy is:

$$COE = \frac{FCR\ x\ ICC}{AEP_{net}} + AOE \tag{2.8}$$

where:

- COE = Levelized Cost Of Energy ($\frac{\$}{kWh}$)
- FCR = Fixed Charge Rate
- ICC = Initial Capital Cost
- AEP_{net} = Net Annual Energy Production
- AOE = Annual Operating Expenses

From the designer's viewpoint, the advantage of this model is that it allows to evalute the economic impact of specific design strategies, by taking into account all the aspects of the operational life of the machine. In fact, each of the members of the equation (2.8) is computed from further contributions which, starting from the values of the design variables, can calculate the impact of each single components to the total cost of energy. For brevity, a detailed description of the cost model is not illustrated here, even because a great research effort is still ongoing in order to refine the model and make the estimate of the cost of energy more accurate. Another advantage of this model is that it allows the optimization to act effectively on all the different parameters affecting the cost, that is, the optimization will pursue an increase in the AEP as much as a decrease in blade weight, which makes the cost of energy more suitable for optimization purposes than other traditional objective functions exploited in the past.

Constraints

The choice of the active constraints that should be included in the optimization process is an important step of the algorithm development, especially because they should represent a good choice of compromise between simplicity and completeness. The certification of modern wind turbines is regulated by international standards [8],[9] which require to test the machine under a variety of circumstances, which are summarized in several design load cases, DLC. They include normal operating conditions, ultimate loads from storm, emergency shutdown and full-turbulent flow simulations. Obviously, an accurate verification of the DLCs requires detailed aero-elastic models coupled with unsteady aerodynamic models, as illustrated in the already cited paper [2]. Since this level of detail goes beyond the scope of this work, in our algorithm we introduce some constraints which can be considered as simplified load cases. The scope is to maintain a strict compliance with the required verifications, without the burden of simulations and analysis required to a commercial software. Specifically, the simplified load cases taken into considerations are translated into the two following constraints:

- **Operating conditions: the first flapwise frequency must be higher than the 3P.** This is imposed by the relation:

$$\epsilon_{freq} - \frac{f_{flap} - f_{3P}}{f_{3P}} \leq 0 \tag{2.9}$$

  where f_{flap} is the first flapwise frequency of the blade, f_{3P} is the three-per-revolution natural frequency of the blade, and ϵ_{freq} is the desired clearance between the two. This constraint poses a lower limit on the first flapwise frequency of the blade corresponding to the nominal operating conditions. The goal is to avoid the superposition between the blade frequency and the 3P, which could result in dangerous resonance phenomena. Since the first flapwise frequncy depends largely on the out-of-plane stiffness of the blade, this constraint should regulate the absolute blade thickness and the sizing of the structural elements, especially the spar caps.

- **Storm conditions: the maximum stress must be lower than the admittable stress.** This condition is enforced on each blade section, and drives the sizing of the structural elements so that the optimal blade can withstand ultimate loads deriving from storm conditions. This can be expressed by the relation:

$$\epsilon_{\sigma} - \frac{\sigma_{adm} - \sigma_{Max}}{\sigma_{adm}} \leq 0 \tag{2.10}$$

  where $\sigma_{Max} = max(\sigma_i)$, that is, the maximum stress detected along the blade. Again, ϵ_{σ} is a tolerance that allows the User to set the required degree of safety.

In addition to these constraints, a limit on the maximum tip speed is imposed. This condition, which concerns the design of onshore wind turbines, derives from acoustic considerations: as the rotor speed of the wind turbine increases, the aerodynamic and mechanical noise can reach high levels, affecting the surrounding environment in a negative manner [10]. This is true especially for megawatt-size machines, which are characterized by great tip velocities. To respect the regulation in force for this class of machines, it is imposed that the tip velocity can not overcome a certain value, which is usually set equal to $72\frac{m}{s}$:

$$\begin{aligned} v_{tip_{max}} &\equiv 72\frac{m}{s} \\ \Omega_{max} &= \frac{v_{tip_{max}}}{R} \end{aligned} \tag{2.11}$$

From the (2.11), it is possible to notice that this requirement affects the maximum rotor speed and, in turn, the regulation strategies and the production of energy. Dislike (2.10) and (2.9), which are explicitly verified by the optimizer at each iterate, the tip-speed constraints is implicitly imposed when the regulation trajectories of the machine are computed.

Design variables

The array of the design variables is defined as the set of the degrees of freedom, that is, it stores all the parameters which are directly controlled by the optimization. In order to grant that all the searchable domain is explored, the array should include several groups of variables, which are related to the different sub-problems of Figure 2.2. In this work, the design variables must include the geometrical description of chord and twist, as much as parametes related to an arbitrary number of airfoils. A description of the various structural elements must also be included in the set of the design variables. Let $\boldsymbol{x}$ be the array of the design variables, it can be considered composed by four families of variables as follows:

$$\boldsymbol{x} = [\boldsymbol{x}_{ch}\ \boldsymbol{x}_{tw}\ \boldsymbol{x}_{st}\ \boldsymbol{x}_{af}] \tag{2.12}$$

where:

- $\boldsymbol{x}_{ch} = [x_{ch}^1, ..., x_{ch}^{n_{ch}}]$ includes the n_{ch} variables related to the chord description.
- $\boldsymbol{x}_{tw} = [x_{tw}^1, ..., x_{tw}^{n_{tw}}]$ includes the n_{tw} variables related to the twist description.
- $\boldsymbol{x}_{st} = [x_{st}^1, ..., x_{st}^{n_{st}}]$ includes the variables related to the thickness of the structural elements.

- $\boldsymbol{x}_{af} = [x_{af}^1, ..., x_{af}^{n_{af}}]$ includes the variables related to the shapes of the airfoils.

the next Chapter illustrates how the design variables are chosen in order to represent the blade shape in a high fidelity manner.

2.3 Project Road-Map

The development of the program follows a step-by-step methodology. As stressed out in the Introduction, while optimization solvers are common in wind energy, no previous application of the integrated blade/airfoils approach has been explored. In order to tackle the problem in a gradual and organized way, the total amount of work has been subdivided in five Work-Packages, in order to investigate gradually the various aspects of the methodology. Figure

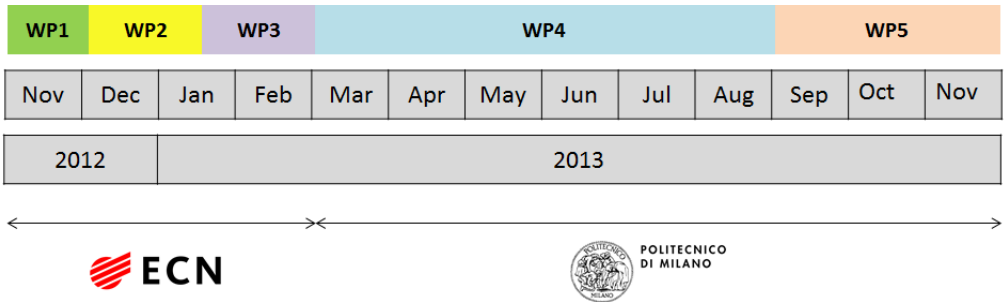

Figure 2.3: Organization and timeline of the project.

2.3 shows the subdivision of the total work amount during the entire duration of the project, namely:

- **WP-1:** Study of available airfoil parameterizations and development of a 2D airfoil optimization tool.
- **WP-2:** Creation and validation of an algorithm for 3D blade performances estimation. Optimization of chord/twist with reference to different objective functions.
- **WP-3:** Integrated 2D/3D aerodynamic optimization of the blade.
- **WP-4:** implementation of the multi-disciplinary approach by including a detailed structural model in the optimization program.
- **WP-5:** Validation of the algorithm with third-part softwares. Case studies performed on several wind turbines, in order to test the capabilities of the free-form methodology.

As illustrated in the picture, WP-1, WP-2 and partially WP-3 were developed at the headquarter of ECN in Petten, the Netherlands, under the supervision of Dr.Grasso. WP-4 and WP-5 were conducted at the *Poli-Wind* unit at Politecnico di Milano, under the supervision of Prof. C.L. Bottasso and Prof. A. Croce. The goal of this kind of organization was to exploit the great experience gained in the past years by both ECN and Politecnico in the field of optimization of Multi-MW class Wind Turbines.

Chapter 3

Mathematical Models

This Chapter provides a survey of the various mathematical models employed in this work. The presentation is divided in three main sub-problems: the 2D aerodynamic description of the blade, the estimation of the 3D aerodynamic characteristics and the structural problem. For each sub-problem, the choice of the design variables is discussed, together with the numerical methods adopted for its solution. The scope is to offer a detailed view of the algorithm capabilities, and to understand the hypothesis and assumptions made at each level of the optimization process.

3.1 Two dimensional aerodynamics

3.1.1 Airfoils description

The representation of the airfoils plays a crucial role within the free-form approach here investigated. The fact that the airfoil shapes are now included as design variables adds some complexities to the already tangled problem of blade optimization. Let's consider, for example, that in state of art algorithms the airfoil data are often provided from wind tunnel measurements. When the airfoils are unfrozen, like in the free-form approach, the estimation of aerodynamic data at each iterate must be done by a numerical method which must replace the wind tunnel experiments, possibly with a high level of accuracy. Moreover, as introduced before, having free airfoil geometries introduces a significant number of additional variables in the optimization. It follows that to avoid an unbearable computational time, it is fundamental to describe the airfoil shapes through some parameterization.

Bézier curves This theory for curves representation is due to Dr.Pierre Bézier, who first introduced this formulation inside Renault in 1960. Subsequently, Bézier curves knew a wide expansion, especially in CAD softwares and in the field of

graphic design. Due to its simplicity, these curves are suitable for representing a wide variety of geometric shapes, as much as complex curves with multiple curvatures. Like other parameterizations, the continuous curve is built from a control polygon, which is constructed by connecting a set of control points with segments. In the domain of the Bézier parameterization, a N-degree curves needs N+1 control points to be defined. Figure 3.1 shows examples of 3^{rd} order Bézier curves.

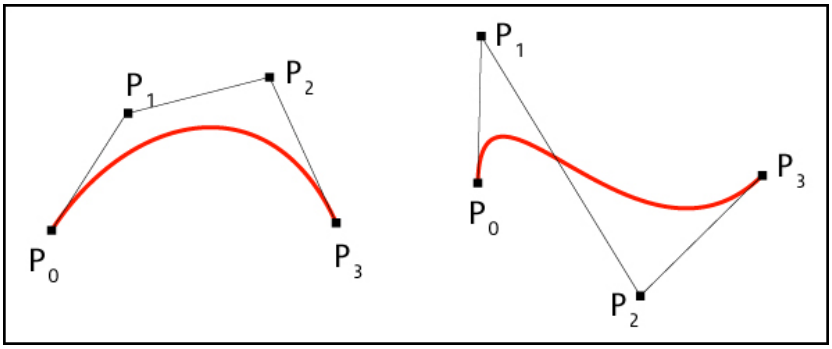

Figure 3.1: Cubic Bézier curves and control polygons.

Among the advantages of this formulation is that a Bézier curve mimics the shape of its control polygon, passes through its first and last control points, and is tangent to the control polygon at those endpoints and, as a consequence, at least two control points of the Bézier belong to the curve. This is appreciated in optimization, because it helps to obtain a stronger connection between the design variables and the underlying curve, thus limiting ill-conditioning problems, which are common in gradient optimization. Matematically, a Bézier curve of order n can be defined by the following relation:

$$\boldsymbol{P}(t) = \sum_{i=0}^{n} B_i^n(t)\boldsymbol{P}_i \tag{3.1}$$

where $\boldsymbol{P}_i$ represent the coordinates of the i-th control point, and B_i^n is the i-th *Bernstein coefficient*, which takes form:

$$B_i^n(t) = \binom{n}{i}(1-t)^{n-i}t^i, \quad i = 0, 1, ..n \tag{3.2}$$

and:

$$\binom{n}{i} = \frac{n!}{i!(n-1)!} \tag{3.3}$$

is the binomial coefficient.

The idea of describing airfoils with the Bézier curves was discussed in several

works from ECN [11],[12] and the parameterization proved to work well within optimization purposes. Here, this methodology is adopted and tailored to suit the needs of the free-form approach. Specifically, the geometry of each airfoil is described through four different third-order Bézier curves, each of them is described by four control points, so that each airfoil is theoretically defined by 16 control points. However, in order to grant continuity, both the upper and the lower surfaces are described by a pair of curves, which are linked together at the point of maximum thickness, so that one curve terminates where the second begins. The upper and the lower surfaces are also connected at the leading edge, so that the actual number of different control points is reduced to 13, as shown in Figure 3.2.

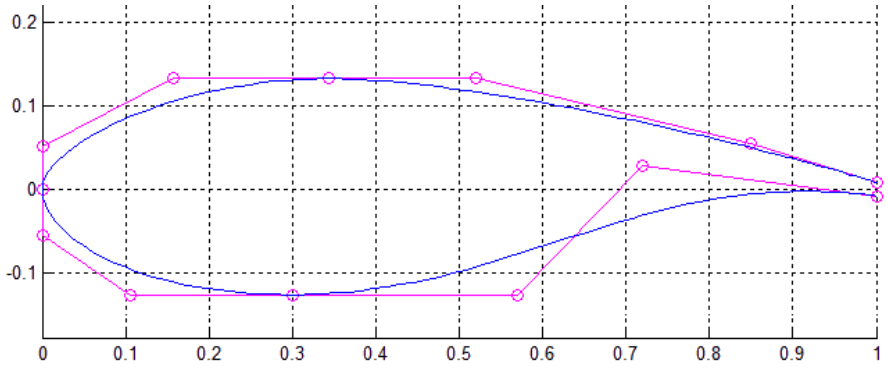

Figure 3.2: Airfoil geometry description with the Bézier curves.

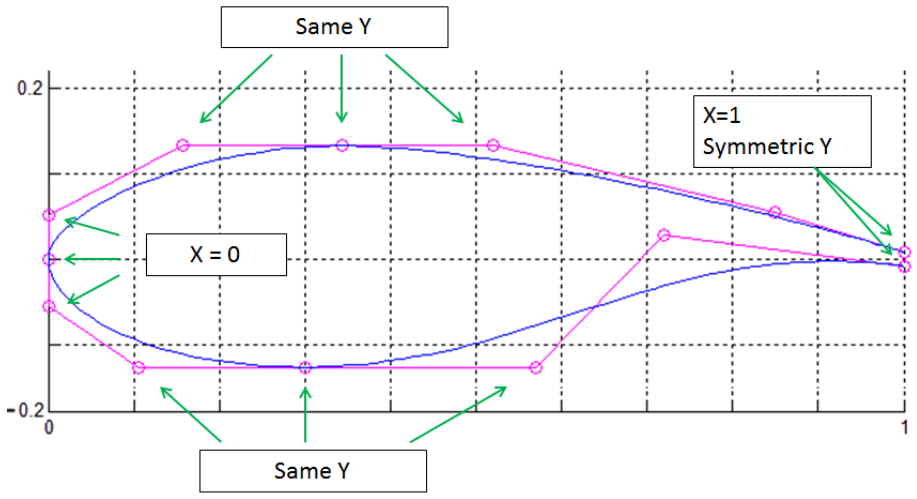

Figure 3.3: Geometric constraints for airfoil description.

One of the main features of the Bézier curves is that they rely on a rather simple analytical formulation, which makes Béziers much more advantageous than other common parameterization employed in arifoil description, like for example the

PARSEC, which requires highly nonlinear equations to be solved in order to estimate the airfoil shape[13]. At the same time, due to its flexibility the Bézier formulation allows a great variety of airfoils to be explored. Within the purposes of this work, for example, it is possible to obtain geometries which are commonly employed in modern wind turbines, like flatback airfoils and S-tail trailing edge for rear-loading. Obviously, such a broad domain can result in strange airfoil shapes appearing during the optimization. In the worst cases, the two-dimensional solver can fail to converge, if the geometry is not smooth enough to allow panel methods to be employed. To avoid this situation, a great care has been taken in order to figure out a set of geometric constraints, which are illustrated in Figure 3.3. This puts some limits in the freedom enjoyed by each control point, forcing each pair of curves to have the same tangent at the connecting point, in order to guarantee that all the curves are merged in a regular and smooth way. As it is evident from the figure, this control does not act at the trailing edge, where the upper and the lower surfaces terminate on different points, in order to allows flatback airfoils. After accounting for the geometric constraints, the number of necessary degrees of freedom for describing each airfoil is 15, which assures enough freedom to allow the representation of a wide range of existing airfoils (DU, FFA, Risø) with a high level of fidelity.

3.1.2 Numerical computation of airfoil data

As outlined in the introduction, typical three-dimensional solvers employed in wind turbines optimization are based on a combined 2D/3D approach. This means that, in order to estimate the three-dimensional aerodynamic performance of the blade, and thus the energy production, it is necessary to provide informations about the local characteristics of the airfoils, typically the lift, the drag and the pitching moment for one or several Reynolds numbers. As the airfoils vary during optimization, it is necessary to provide those values numerically, in the entire range of angles of attack encompassed between $\pm 180°$. In our algorithm, this is done as follows: at first, each airfoil is evaluated in the range $\pm 20°$ with the popular solver `XFOIL` [14] then, a numerical implemetation of the Viterna-Corrigan method extends the data collected from `XFOIL` to the whole range [15]. This strategy has been previously adopted for the optimization of wind and tidal turbines dedicated airfoils, as illustrated in [16]. While the details of the models can be found in the references, it is our interest here to provide a brief summary of the capabilities of `XFOIL`. In particular, the program provides:

- An inviscid formulation, based on a simple linear-vorticity stream function panel method, completed with the forcing of the Kutta condition at the trailing edge
- A Karman-Tsien compressibility correction which allows good compressible predictions until the appearence of the sonic conditions

- A viscous formulation, which relies on a two-equation lagged dissipation BL formulation and a e^n transition criterion.

The coupling between inviscid and viscous formulations allows to perform a variety of analysis which go further the estimation of lift, drag and moment at a certain angle of attack. However, as stressed out in the documentation, the program provides reliable results only in the pre-stall region, where a good agreement with experimental data is usually obtained. In Figure 3.4 wind tunnel data for the NACA 1412 airfoil are compared against a viscous simulation performed with `XFOIL`. Both the data series refer to a Reynolds number of 3 millions [17].

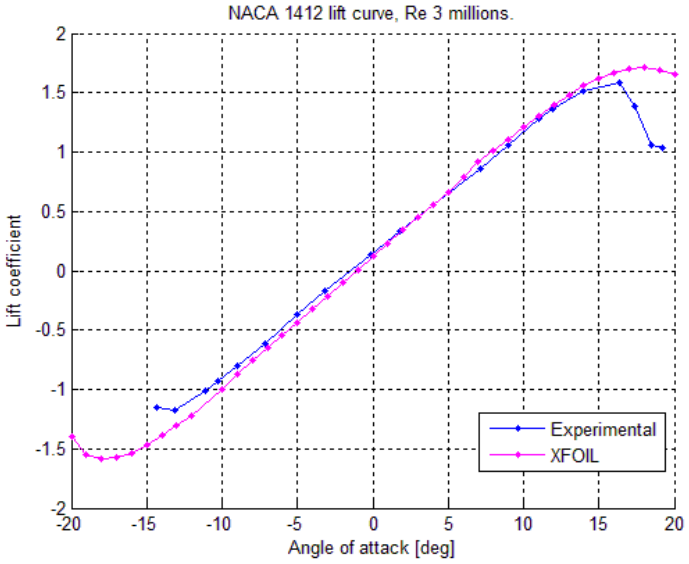

Figure 3.4: Comparison between experimental data and viscous XFOIL simulation for NACA 1412 airfoil.

As it is evident, `XFOIL` fails to describe the near-stall and the post-stall regions and, generally, it computes a significant higher lift. The dual situation happens for the negative stall, where a lower lift is computed. This peculiar beahviour must be handled with care, as it puts a serious limit on the usage of `XFOIL`, and panel methods in general, for the evaluation of wind turbines airfoils. In fact, usually a full characterization of the stall region is required in order to gain a full overview of the aero-elastic behaviour of the blade, as stall-induced vibrations could trigger flutter mechanisms [18]. In this work, where aeroelasticity is not accounted for and where the aerodynamics is considered steady, this is not a relevant problem. Vice versa, a more striking consideration concerns the Viterna model, which basically makes use of the flat plate theory in order to extend the airfoil data from the region after stall to the entire range of angles of attack. An example of the typical resulting curves for the lift and the drag coefficients is shown in Figure 3.5.

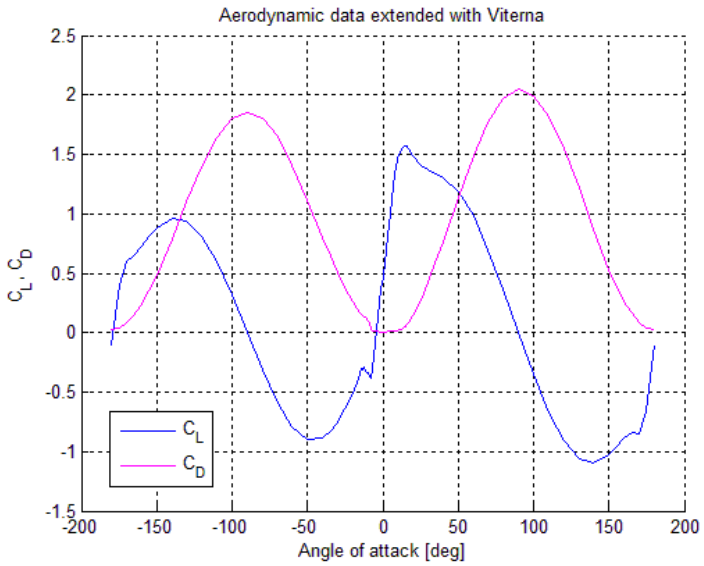

Figure 3.5: Example of aerodynamic data extended with Viterna-Corrigan model

Obviously, more accurate data result in the Viterna curves to better fit the experimental data, and this is true especially for the stall region, where the curve of the available data is connected with the Viterna extension. As a consequence, the use of `XFOIL` will definitely put some limits in the accuracy of the Viterna curves, and future developments of the work should consider an improved methodology for the estimation of two-dimensional airfoil performances.

3.2 Three dimensional aerodynamics

3.2.1 Blade description

The description of the aerodynamic part of the blade, is done essentially by defining the chord function and the twist function. For optimization purposes, it is necessary to adopt a parameterization, so that a reduced number of degrees of freedom can control effectively the entire design. In this work, chord and twist are defined along the blade by means of the same Bézier curves introduced in 3.1.2. Figure 3.5 shows the non-dimensional chord function of a megawatts-size wind turbine described by a Bèzier curve of order five, which means that 6 control points are needed for the description of the entire blade. It must be pointed out that control points 1 and 6 are considered frozen for geometric purposes. This implies that they not participate in optimization, so that the number of degrees of freedom related to the chord is eight, correpsonding to the set of coordinates $[x_i, y_i]$ for $i = 2, ..5$.
The description of the twist function follows the same rule: also in this case a

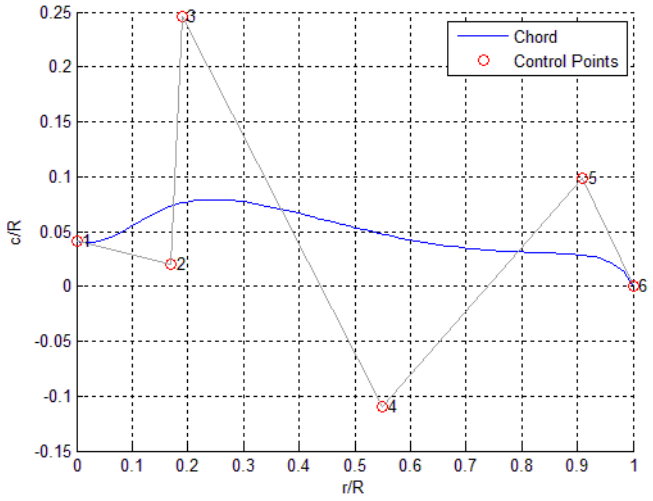

Figure 3.6: Chord function described by a 6^{th} order Bézier curve.

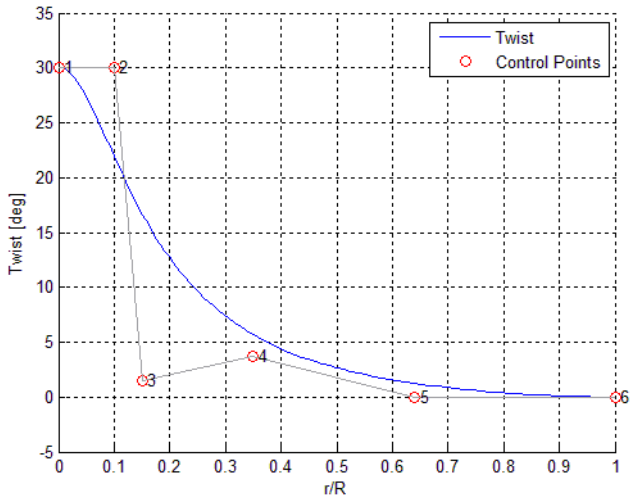

Figure 3.7: Twist function described by a 6^{th} order Bézier curve.

5^{th} order Bézier curve is used and, again, control points 1 and 6 are considered frozen, so that 8 degrees of freedom are related to twist. An example of the parameterization is given in Figure 3.7.

A set of airfoils needs to be assigned along the blade span. Usually, the hub region is equipped with a cilindrical section, which serves as connection with the bearings system. Sometimes particular transitional airfoils are also present, in order to facilitate the passage from the cylindrical area to the rest of the blade, which is equipped with regular airfoils. From an aerodynamic point of view, there is no convenience in optimization of the region close to the hub, as

its contribution to the overall power production is neglectable, and the design is driven by structural considerations. Moreover, bizarre airfoil shapes like ellipsoids or cylinders may cause `XFOIL` to crash. To avoid this, in the free-form algorithm each airfoil can be listed as *active*, if it will be included in the optimization, or *frozen*, if not. In the latter case, it is necessary to provide aerodynamic data for the frozen airfoils, like any other blade optimization tools. An example of the assignment of the airfoils along the blade is shown in Table 3.1, in a simplified fictional case where only four airfoils are investigated.

Table 3.1: Example of airfoils distribution along the blade

Active	Airfoil	Thickness %	Position
0	Airfoil 1	100	0.0
1	Airfoil 2	40	0.32
1	Airfoil 3	30	0.75
1	Airfoil 4	25	1.00

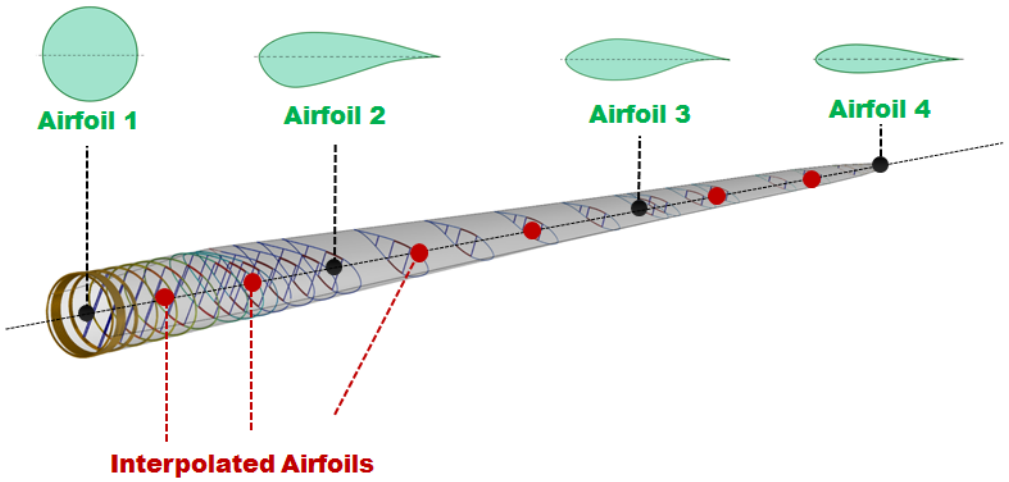

Figure 3.8: Interpolation of airfoils.

In this case the first airfoil, here referenced generally as Airfoil 1 but usually a cylinder or similar, is not involved in the optimzization, while the rest of the airfoils is. The User can assign an arbitrary number of active airfoils and an arbitrary number of frozen ones, as long as he/she has aerodynamic data available for them. It is important to notice that each airfoil is assigned to a specific coordinate, which is given as a non-dimensional radial position. The aerodynamic and structural properties of intermediate airfoils are obtained by interpolation, as depicted in Figure 3.8, which assures that an arbitrary number of sections can be considered for the three-dimensional simulation.

3.2.2 AEP computation

The annual energy production, AEP is the quantity that yields the contribution of the aerodynamic performance of the blade within the objective function. In this work, the three-dimensional aerodynamics is treated with an open-source solver based on a standard BEM theory, for which the details are reported in [19]. The solver is able to analyze straight, twisted and tapered blades, and several features of the rotor can be taken into consideration, like yaw, tilt and cone angles. The model of the wind is extremely simplified, as it is considered steady across the rotor, but allows to define an exponential shear factor to take into account possible non-uniformities of the incoming wind field. Such a simple model, coupled with some intrinsic limits in the BEM formulation, would surely lead to over-extimation of the blade performances. For this reason, the Prandtl tip correction is included in the model, together with the hub correction for heavy-loaded wind turbines. At each iterate, the computation of the AEP is done following these steps:

- Computation of the *Cp-Lambda* curves for determination of the optimal conditions
- Application of the regulation strategies and generation of the power curve
- Application of the Weibull distribution, in order to adapt the power curve to a particular wind site.

At first, then, a BEM analysis is run, in order to determine the envelope of the *Cp-Lambda* curves.Figure 3.9 provides an example of these curves, which are typically computed for a discrete set of TSR and pitch values. The resulting envelope is treated with a surface interpolation technique, in order to refine the accuracy of the mesh. Since BEM is not errors-proof, a great care was taken in order to prevent and possibly bypass fatal crashes of this module, by the programming of errors-detection safety circuits for the avoidance of program breakdowns.

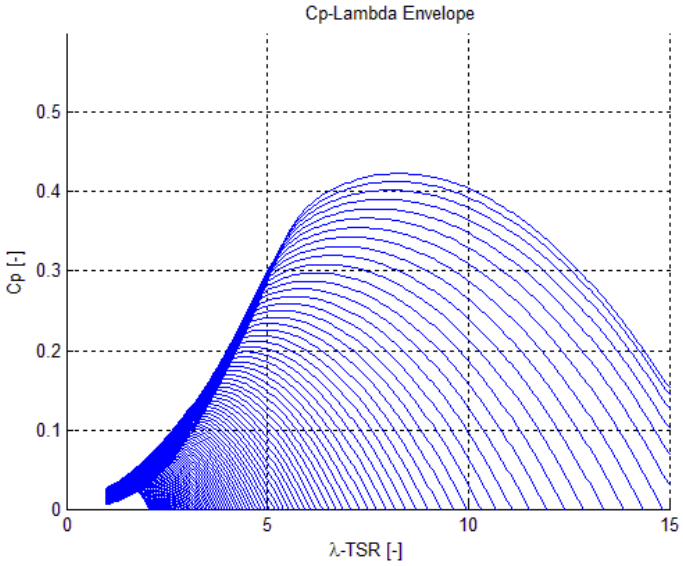

Figure 3.9: Cp-lambda curves.

From the Cp-lambda curves, the power generation curve can be computed in the operating range of wind speeds $[V_{cut_{in}}\ V_{cut_{out}}]$. In the algorithm, this is obtained by means of the classical regulation strategies which govern the power production of a pitch-regulated, variable speed wind turbine.Basically, these imply a constant TSR strategy for the region 2, below the rated power, and a constant power strategy for the region 3, above the rated power. For onshore wind turbines, where the noise emissions must fulfill a strict regulation, it is possible to impose a limit on the tip speed in order to reduce the acoustic impact on the surrounding environment. This limits also the rotor speed and modifies the implementation of the regulation trajectories, giving birth to an intermediate region $2\frac{1}{2}$ where a constant speed strategy must substitute the classical constant TSR strategy. The different regulation trajectories are summarized below, while the resulting power curve is illustrated in Figure 3.10.

- Region 2: constant TSR strategy

$$\begin{aligned} C_p &= C_p^* = max(C_p(\lambda, \beta)) \\ \lambda &= \lambda^* \\ \beta &= \beta^* \\ P &= \frac{1}{2}\rho A V^3 C_p^* \\ \Omega &= \frac{V\lambda^*}{R} \\ T &= \frac{1}{2}\rho A R V^2 \frac{C_p^*}{\lambda^*} \end{aligned} \tag{3.4}$$

- Region $2_{\frac{1}{2}}$: Constant speed strategy

$$\begin{aligned}
\Omega &= \frac{V_{tip-max}}{V} = \Omega_{max} \\
\lambda &= \frac{\Omega_{max} R}{V} = \lambda(V) \\
C_p &= max_{\beta}(C_p(\lambda(V), \beta)) \\
\beta &= argmax_{\beta}(C_p(\lambda(V), \beta)) \\
P &= \frac{1}{2}\rho A V^3 C_p \\
T &= \frac{1}{2}\rho A R V^2 \frac{C_p}{\lambda}
\end{aligned} \tag{3.5}$$

- Region 3: Constant power strategy

$$\begin{aligned}
\Omega &= \Omega_{max} \\
\lambda &= \frac{\Omega_{max} R}{V} = \lambda(V) \\
P &= P_{Rated} \\
C_p &= \frac{2 P_{Rated}}{\rho V^3 A} \\
\beta &= \beta(C_p, \lambda) \\
T &= \frac{1}{2}\rho A R V^2 \frac{C_p}{\lambda}
\end{aligned} \tag{3.6}$$

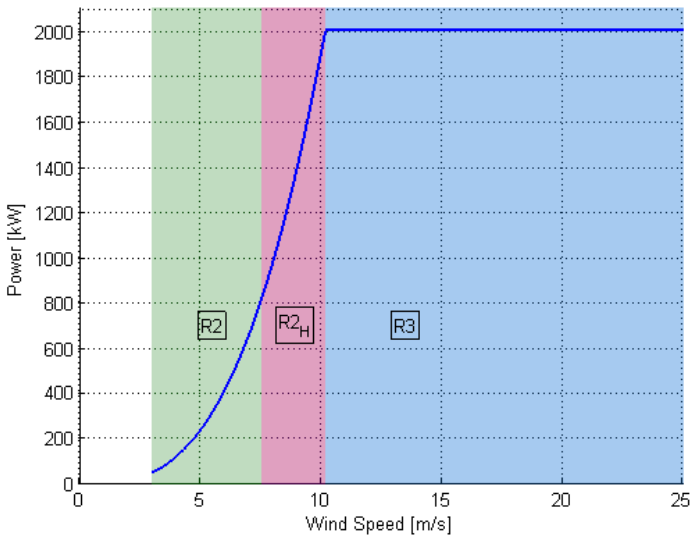

Figure 3.10: Power Curve.

The computation of the annual energy production requires to adapt the power curve to the particular wind site under consideration. This is done by weighting the power curve with the Weibull distribution, whose probability density function is defined as:

$$f(V) = \frac{k}{\lambda^k} V^{k-1} e^{-(\frac{V}{\lambda})^k} \tag{3.7}$$

where V is a the wind speed, $k \in R$ is the *shape factor* and $\lambda \in R$ is the *scale factor*. The use of the Weibull distribution is common in wind energy, since through the shape and scale paramteres it is possible to fit statistical data of most real sites. An example of various applications of the Weibull is provided in Figure 3.11. Here the function is defined up to $5\frac{m}{s}$ for clarity but, obviously, for proper AEP computation the function must be defined in the whole operating range $[V_{cut_{in}}\ V_{cut_{out}}]$.

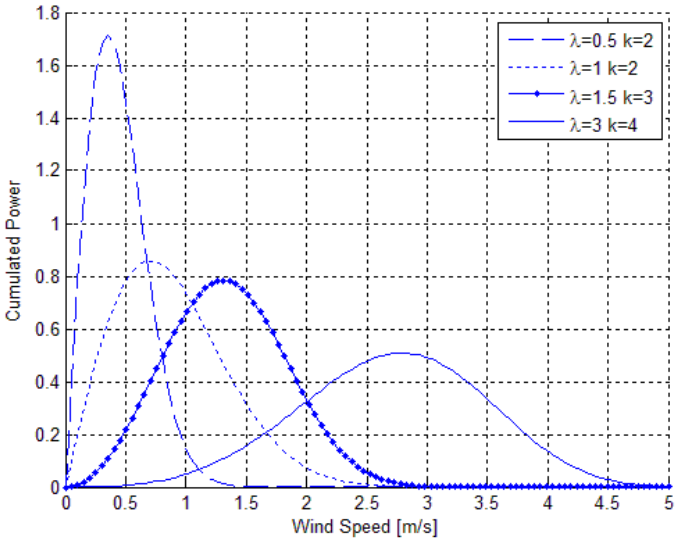

Figure 3.11: Weibull distribution.

3.3 Structural analysis

As it was discussed earlier, a multi-disciplinary approach towards blade optimization must account for all the relevant aspects of the wind turbine design. While the aerodynamic design of the blade is responsible for the power production, the structural design must address the important topics of efficiency and safety and, as a consequence, the sizing of the structural elements must be carried out in good fulfillment with international guidelines [9], which include a set of design load cases, DLCs, for the certification of wind turbines. Generally, the structural and safety design is driven by fatigue loads considerations, as much as ultimate

loads analysis and instability avoidance, when complex aero-elastic models are available. In this work our intention is to favour simplicity: the main scope is not do develop a commercial code but rather to explore the implications of the free-form methodology and, for this reason, we chose to employ simplified versions of DLCs, which result in the two constraints illustrated in section 2.2. In the following, the models which constitute the structural simulations are discussed.

3.3.1 Description of the blade section

The internal arrangement of the structural elements is a main topic in wind turbines design. Most of the early solutions adopted in wind energy were derived from aerospace applications, since the load spectrum to be applied with respect to fatigue strength, and the mathematical methods for the dimensioning of the structure, which is highly stressed dynamically, are both similar. Nevertheless, the design of a wind turbine is heavily affected by considerations about cost of energy, and this makes borrowing from aircraft engineering only possible to a limited extent, because of the much narrower cost margin which prohibits the application of traditional aircraft manufacturing methods. At present, several manufacturing techniques are available for the realization of the internal structure. A complete survey of them is provided in most wind energy texbook, for exemple in [20]. In this work, we assume a three-cells box section which is based on the *stressed shell* approach, a common solution employed in large wind turbines which is exemplified in Figure 3.12.

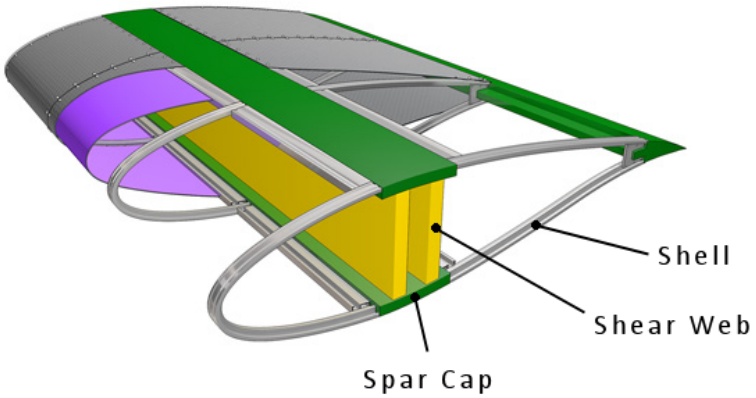

Figure 3.12: *Stressed shell* blade section.

The ideal section is made up of three essential elements:

- A skin shell, whose main task is to preserve the aerodynamic shape. It also

plays a structural role in stiffening and strengthening the spar, particularly to resist torsion (twisting) loads.

- Two spar caps, which bear the significative bending moment acting along the blade.
- Two shear webs which are connected to the other elements in order to grant the required shear strength.

This formulation is quite essential and it simplifies the actual techniques of blade construction. Thus, some aspects of the manifacture are neglected like, for example, the fact that usually the shear webs are made up of composite layers filled with foam or a core material, in order to prevent *buckling* phenomena due to a high compressive stress. Modern blade sections are also equipped with leading edge and trailing edge reinforcements in order to increase the in-plane stiffness. However, it must be noticed that the constraints employed in this work concern mainly the out-of plane deflections and the stress in the spar cap, for which the simplified structure adopted is perfectly adequate. It should be easy, in future developments, to introduce a more accurate description of the blade section, in order to account for buckling verification or torsional stress evaluation, if needed.

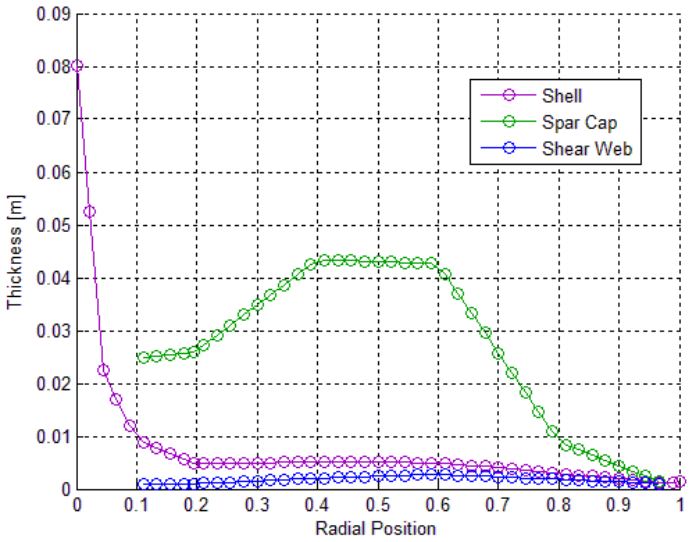

Figure 3.13: Thickness of structural elements.

Figure 3.13 shows the typical distribution of thickness of the various elements along the blade. Basically, the shell is defined along the entire blade and shows a peak near the hub, where a great thickness is required in order to lodge the connections with the hub. For the optimization purposes, the thickness of the shell and the shear webs is maintained constant, since no controls of torsion or

buckling are currently present in the program, and leaving them free to change could lead to an overestimation of the structural performances. On the contrary, the spar cap thickness is left free to optimization, and the User can specify an arbitrary number of degrees of freedom related to the spar cap thickness in order to tune the sensitivity of the optimization to his/her goals.

3.3.2 Finite Elements Methods for structural analysis

The numerical evaluation of the blade structure is usually addressed with a beam scheme. However, the complexity of the internal configuration and the fact that composite materials are employed for manifacture require some additional care when trying to choose the best model for structural description. The idea of employing Finite Elements in wind turbines blade description is extensively illustrated in [21], where a full three-dimensional FEM method is proposed for the structural evaluation of the blade. In the context of this work, it must be kept in mind that the airfoils are expected to change continuosly, as the optimization go on, and this brings serious implications even in the structural aspects of the design, as the absolute thickness of the blade change accordingly. Looking at the constraints, summarized by the relations (2.9) and (2.10), we see that at each iterate it is necessary to compute the local (normal) stress acting in the various sections and the first flapwise frequency of the blade. The aerodynamic loads deriving from ultimate storm conditions represent the forcing term, thus achieving a full aero-structural coupling within the blade description. As the blade weight influences directly the computation of the objective function, an accurate computation of the distributed masses is also required. In order to follow simplicity, but also in a vision of computational time saving, the introduction of a 3D FEM description is delayed to future developments of the program and, for the time being, the structural evaluation is performed by coupling a 1D beam model with a local 2D cross-sectional solver. The conceptual workflow of the structural analysis is illustrated in Figure 3.14, where the various steps are represented by individual blocks. The computation of the aerodynamic loads is reported outside the main block, since it is not part of the proper structural analysis, but is must rather be seen as the application of a forcing term.
Hence, the global description of the blade is obtained by a 1D cantilevered-beam model, which is employed for the computation of the blade frequencies, as illustrated in [22]. The solver is BModes from NREL, which uses a finite-element approach in conjunction with analytical linearization and a special finite-element assembly that captures Coriolis and centrifugal effects. Its finite-element approach is based on a 15-dofs element with three internal and two boundary nodes, as illustrated in Figure 3.15. The 15 dofs comprise 3 dofs for torsion deflection and 4 dofs each for axial, flap, and lag deflections.
It must be noticed that, following this approach, the coupling between the structure and the aerodynamic design is doubled as the operating rotor speed Ω enters

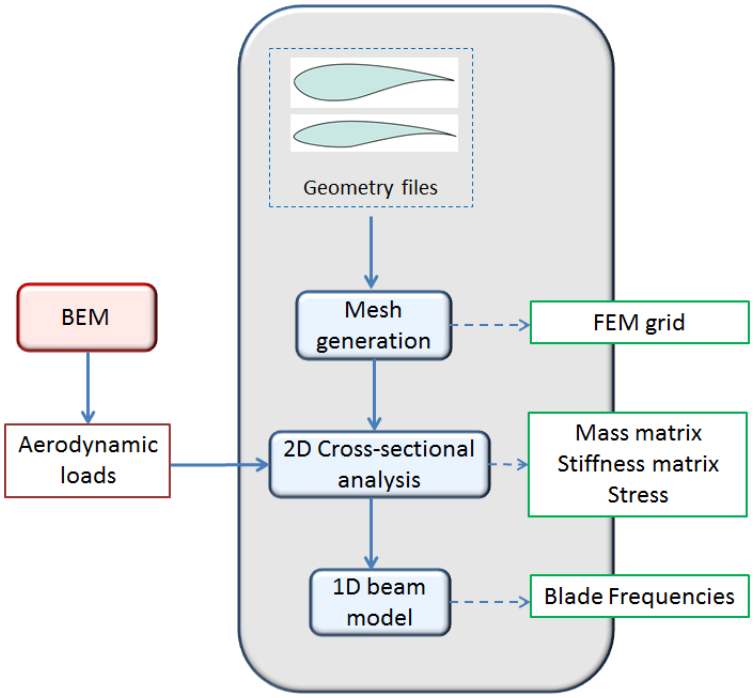

Figure 3.14: Structural simulation workflow.

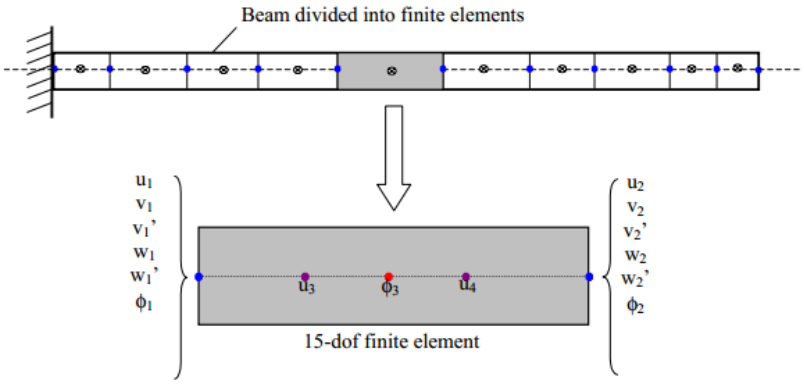

Figure 3.15: Beam discretization into 1D finite elements.

in the computation of the vibrating modes. In order to process the blade with BModes, span-wise sectional properties are required. They include flap-wise and edge-wise mass and stiffness, as much as informations about the locations of the shear center and the elastic center and the inertial properties of each section. In this work, this is done by evaluating each section with a 2D surface Finite Elements solver, as reported in Figure 3.14. The complexity of the manufacture requires to adopt anisotropic and inhomogenous beam models for the evaluation of the cross-sectional properties, for which few validated solvers are currently available. This work exploits `BECAS` [23], which was developed at the Techni-

cal University of Denmark and is largely based on the significant research about anisotropic beams models carried out at Politecnico di Milano over two decades. The interested reader can refer to [24] and [25] for a complete account of the underlying theory.

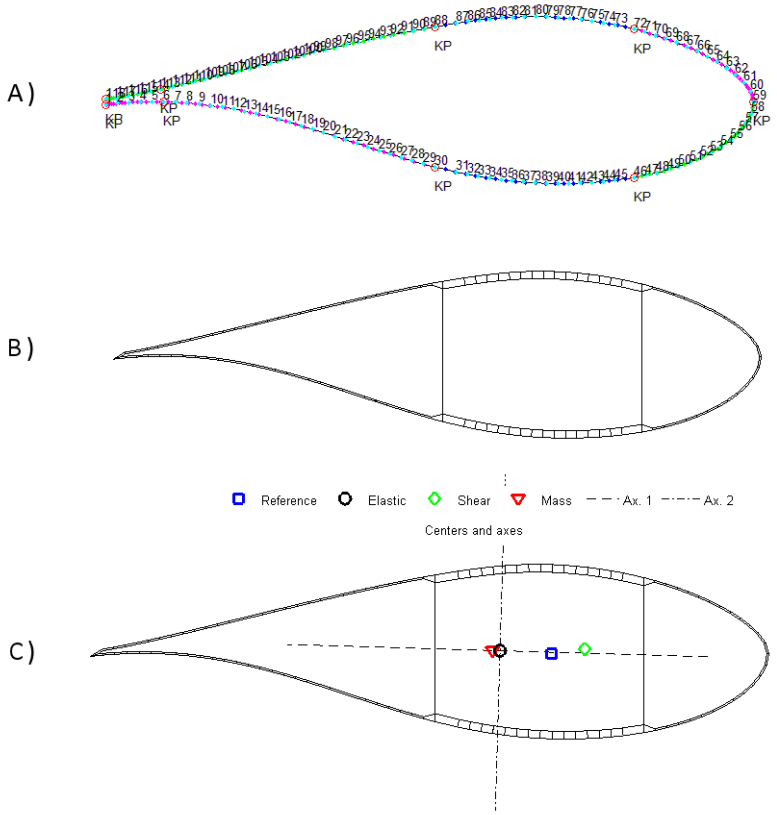

Figure 3.16: Finite Elements analysis. a) Airfoil geometry pivoting, b) Mesh generated by `AirfMesh` and c) typical `BECAS` output.

While `BECAS` provides the solver, it was necessary to write a set of routines for the generation of Finite Elements mesh over sections of arbitrary shape. This led to the development of `AirfMesh`, a preprocessor which is able to take as input an airfoil geometry file, described in Section 3.1.2, and to produce a Finite Elements grid suitable for `BECAS`. The tool was developed by the author, and a great care was taken in order to allow the discretization of all the possible sectional shapes which are generated along the blade including cylinders, open and closed sections, transitional and flatback airfoils. Figure 3.16 shows an example of sectional analysis provided by `AirfMesh` and `BECAS`. The mesh is generated by identifying nine *pivot* points and by projecting each surface along its normal direction. A significant effort has been done in order to obtain smooth connections between

the different elements, in order to preserve a good accuracy of the results.
Considering that the FEM analysis can require a significant computational time when a fine grid is employed, the User is left free to choose the number of Finite Elements to be used for the discretization of each section. A convergence analysis was performed in order to establish the best compromise between accuracy and computational time, and the results for a stiffness-estimation analysis are shown in Figure 3.17. This could be used as a guideline for the determination of a suitable number of Finite Elements: for example, a number of FE equal to 2500 is characterized by an error of about 1.5 % with reference to the convergence solution.

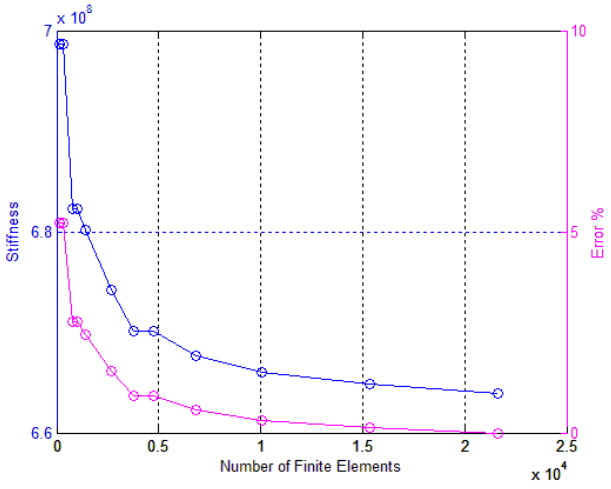

Figure 3.17: Convergence analysis for Finite Elements Method.

3.3.3 Materials

Looking again at the constraints provided by equations (2.9), (2.10) it is straightforward to imagine that the choice of the materials can have severe implications in the optimization process. The formulation with the Finite Elements allows to manage the distribution of the materials in a very precise way, and modern composite materials like Fibre Reinforced Polymers can be handled with a great accuracy. In our model, the User is asked to assign three different materials, one for each structural element, providing mechanical data and informations about fibers orientation, as much as informations about the typology of the material (uniaxial, bi-axial or three-axial composites). As depicted in Figure 3.18, the first material is assigned to the shell, the second is assigned to the spar caps and the third to the shear webs,

Figure 3.18: Assignment of the materials.

As discussed earlier, at present each structural element is considered to be made by a single layer of material. Future developments will bring a more sophisticated structural description, with the possibility to use multiple-layered elements and to assign different materials to the same element.

Chapter 4

Case Studies

In this Chapter, we provide examples of the application of the free-form methodology. The algorithm developed in this work is employed for the optimization of rotor blades taken from real-world machines. The main goals are to validate the program, to assure that it can represent a baseline wind turbine with a satisfactory level of accuracy, and to verify the behaviour of the free-form methodology, in order to understand if it can offer improvements to the traditional optimization strategies.

4.1 Reference 2 MW wind turbine

The first case study concerns a typical megawatt-size wind turbine which, for brevity, will be hereafter referenced as the REF45-2.0 wind turbine. The design was carried out by ECN and Politecnico di Milano, and the features are typical of a modern variable speed, pitch-regulated wind turbine designed for strength. The main features of the wind turbine are listed in Table 4.1.

Class	IEC IIIA
Rotor orientation	Clockwise, upwind
Control	Variable speed, collective pitch
Cut in speed	3 m/s
Cut out speed	25 m/s
Rated power	2.0 MW
Number of blades	3
Rotor radius	46.2 m
Hub Radius	1.2 m
Cone angle	1.0 deg

Table 4.1: REF45-2.0 wind turbine: overall characteristics

The advantage of working with a real reference machine is that it is possible to start the optimization from a good initial point. Since the behaviour of gradient-methods is typically influenced by the initial guess, the use of a high-efficiency initial solution which is the result of a classical aero-structural optimization process makes easier to relate possible improvements with the peculiarities of the free-form methodology. On the contrary, starting from a highly-penalized configuration would tell little or nothing about the actual functioning of the algorithm. For what concerns our purposes, the optimization acts essentially on the blade, and the various properties of the reference blade must be provided carefully, in order to obtain a good representation of the reference machine within the domain of our simplified free-form algorithm. In this context, the essential blade-span properties of a single blade are listed in Table 4.2, while Figure 4.1 and Figure 4.2 show the arrangement of the external and internal layout of the blade, together with the initial thickness distribution of the various structural elements.

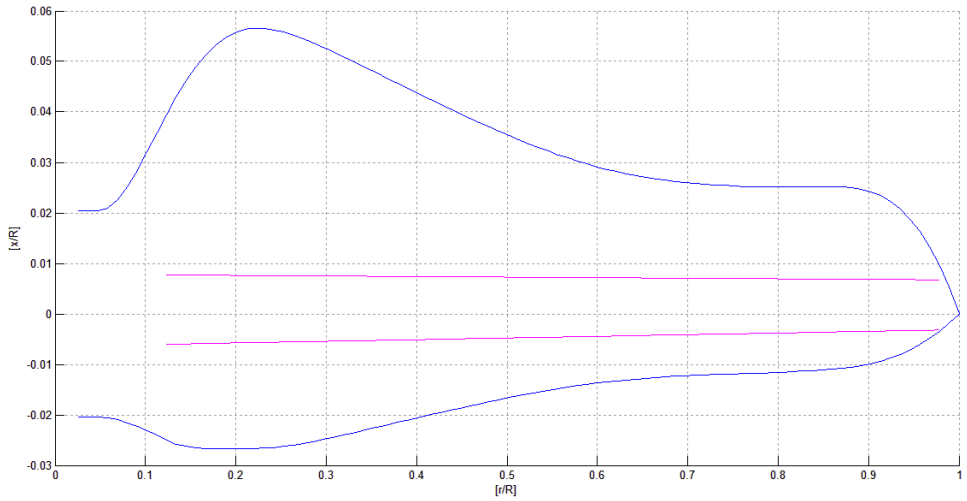

Figure 4.1: REF45-2.0 wind turbine: blade planform and spar cap position.

4.1.1 Optimization set-up

Once the properties of the reference blade are defined, it is necessary to assign a distribution of intial airfoils along the blade, as much as the properties of the various materials assigned to the various structural elements. The reference blade is equipped with highly-efficient DU airfoils, which have been developed at the Delft University of Technology for use on large-sized wind turbines. A discussion on the characteristics of this family of airfoils can be found in [26].

η	Radius	Chord	Twist	E_{11}	E_{22}	Mass
$[-]$	$[m]$	$[m]$	$[deg]$	$[Nm^2]$	$[Nm^2]$	$[Kg/m]$
0	1.20	1.88	18.75	4.66E+09	4.66E+09	849.80
0.0444	3.20	2.01	18.72	1.75E+09	1.97E+09	289.28
0.0889	5.20	2.77	18.36	1.69E+09	1.83E+09	217.81
0.1333	7.20	3.48	17.44	1.35E+09	1.98E+09	181.83
0.1778	9.20	3.80	15.77	1.03E+09	1.87E+09	155.95
0.2111	10.70	3.84	14.10	8.59E+08	1.65E+09	145.88
0.2556	12.70	3.70	11.67	7.07E+08	1.47E+09	150.11
0.3	14.70	3.47	9.44	5.53E+08	1.21E+09	152.18
0.3444	16.70	3.21	7.71	4.19E+08	9.68E+08	153.74
0.3889	18.70	2.95	6.42	3.14E+08	7.63E+08	154.92
0.4333	20.70	2.69	5.47	2.23E+08	5.89E+08	149.52
0.4778	22.70	2.45	4.77	1.57E+08	4.51E+08	142.35
0.5222	24.70	2.24	4.22	1.12E+08	3.48E+08	135.79
0.5667	26.70	2.05	3.71	8.16E+07	2.75E+08	130.03
0.6111	28.70	1.91	3.17	6.06E+07	2.20E+08	120.73
0.6556	30.70	1.82	2.52	4.26E+07	1.70E+08	99.29
0.7	32.70	1.76	1.82	3.04E+07	1.35E+08	79.40
0.7444	34.70	1.72	1.12	2.12E+07	1.08E+08	60.63
0.7889	36.70	1.70	0.46	1.33E+07	8.56E+07	42.62
0.8333	38.70	1.68	-0.10	9.15E+06	6.86E+07	32.42
0.8778	40.70	1.64	-0.51	5.86E+06	5.17E+07	24.59
0.9222	42.70	1.44	-0.62	2.70E+06	2.67E+07	15.97
0.9667	44.70	0.84	-0.27	3.38E+05	4.15E+06	6.47
1	46.20	0.01	0.40	3.28E-03	2.98E-01	0.02

Table 4.2: REF45-2.0 wind turbine: essential blade-span properties

Number	Active	Airfoil	Thickness %	Position $[m]$
1	No	Cylinder	100	1.2
2	No	Cylinder	100	2.2
3	Yes	DU00-W2-401	40	7.0
4	Yes	DU97-W-300	30	14.0
5	Yes	DU91-W2-250	25	19.35
6	Yes	DU93-W-210	21	26.25
7	Yes	DU95-W-180	18	46.2

Table 4.3: REF45-2.0 wind turbine: Initial airfoils distribution.

The original blade has nine different airfoils placed along its span. In this case

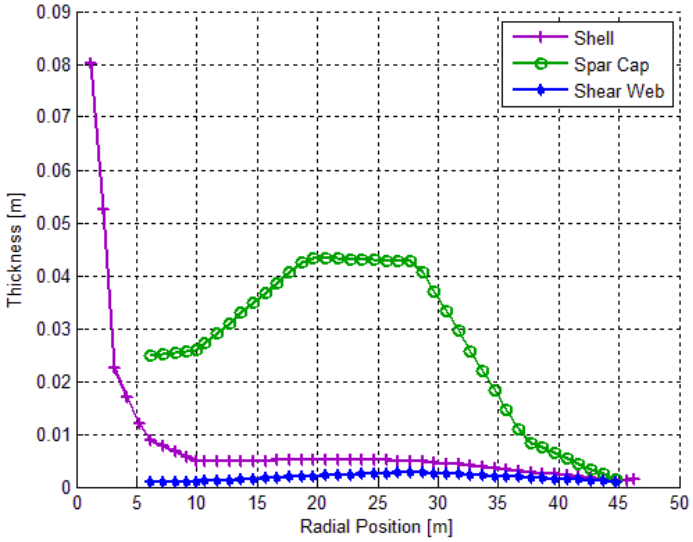

Figure 4.2: REF45-2.0 wind turbine: thickness of the structural elements.

study, however, we must recall that each active airfoil will add 15 degrees of freedom to the total number of the design variables. Then, in order to avoid an extremely long computational time, the configuration has been re-arranged so that only seven airfoils are employed. Table 4.3 shows how the different airfoils are placed along the blade. As shown, the total set of airfoils include two cylinders which are assigned to the hub and which do not take part in optimization and five Delft University airfoils which are left free to optimization. The various geometries of the DU airfoils are obtained from original data and are presented in Figure 4.3. In order to maintain a good coherence between the data and the model, especially under a structural point of view, all the airfoils have been placed so that the relative thickness distribution of the original blade is maintained. This is illustrated in Figure 4.4.

The formulation with the Finite Elements allows to consider multi-directional composite plys within the structural simulation. The properties of the various material were obtained from the individual mechanical properties of the fibers and the matrix as follows: first, the apparent properties of a single unidirectional laminae were obtained following a micromechanical approach [27]. Subsequently, the equivalent properties of the multi-directional plys were derived with the Classical Lamination Theory. Table 4.4 shows the derived mechanical characteristics of the various materials employed in this test.

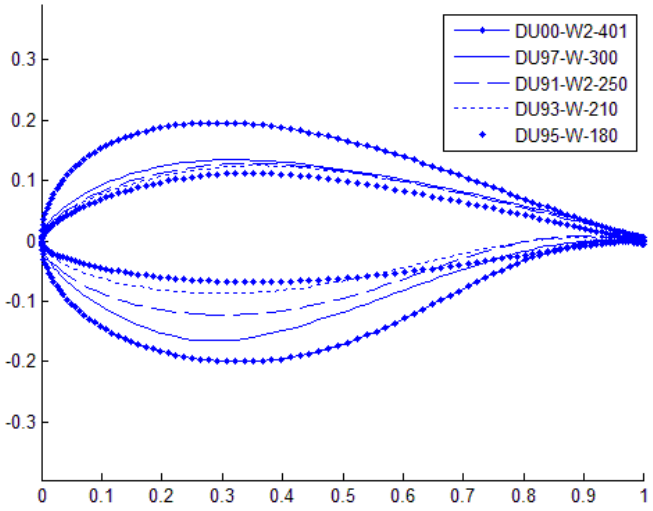

Figure 4.3: Delft University airfoils for wind turbines.

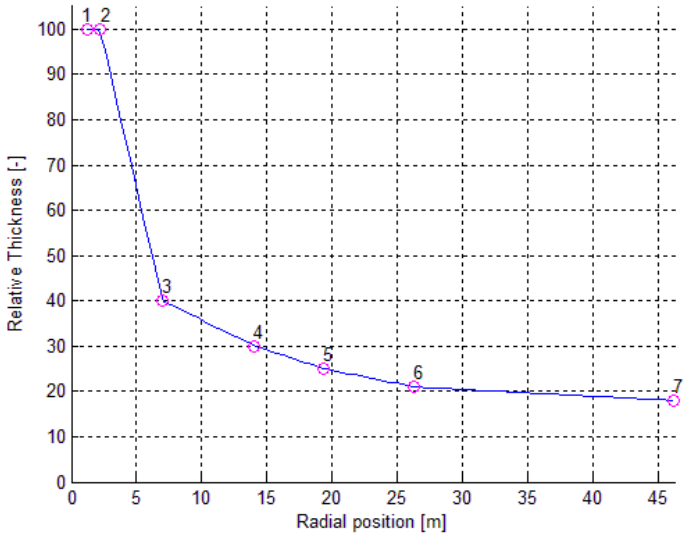

Figure 4.4: REF45-2.0 wind turbine: relative thickness.

4.1.2 Results

The optimization was performed by running the free-form algorithm on a normal personal computer, under Windows and with an i5 processor and 4 gb RAM. The global performaces of the algorithm are reported in Table 4.5.

The optimization process was halted by a convergence criteria, where the convergence of the solution was measured within a tolerance between two subsequent

Material	Element	E_x	E_y	G	ν_{xy}	ρ	$\sigma_{x\ max}$	$\sigma_{x\ min}$
		[MPa]	[MPa]	[MPa]		[Kg/m^3]	[MPa]	[MPa]
Traxial	Shell	28544	10280	6470	0.438	1888	514	-356
Biaxial	Webs	9737	9737	10913	0.596	1874	92	-92
Uniaxial	Spar Caps	38244	8626	3506	0.259	1901	688	-478

Table 4.4: REF45-2.0 wind turbine: Materials.

Total computational time	68.55 hours
Total number of iterates	63
Covergence tolerance	1.0e-8
Value of Frequency constraint at convergence	-6.14e-08
Value of Stress constraint at convergence	-1.22e-03

Table 4.5: Case study 1: algorithm performances.

iterates. We notice immediately that the total computational time is in the order of days, which is comparable against traditional optimization algorithms based on a gradient-method approach. The final value of each constraint is reported. According to the relations (2.9), (2.10) a negative value indicates that the corresponding constraint is satisfied. It is evident from the table that, at convergence, the frequency constraint is very close to zero. On the contrary, the final value of the stress constraint is larger by orders of magnitude, which means that the final design was driven basically by stiffness and frequency considerations.
The global features of the optimal blade are compared against the initial configuration in Table 4.6. The table illustrates the total variation in the cost of energy, together with the corresponding variations in energy production and blade weight. It must be recalled that, since the rotor radius is considered fixed in this simulation, the AEP and the weight are the two major parameters which influence the cost of energy. The evolution of the COE through the various iterates is depicted in Figure 4.5.

	Initial	Optimal	Gain
Cost of energy [$/kWh]	0.047565679	0.04682044	1.57%
Annual Energy Production [kWh/yr]	8006920	8106052	1.24%
Blade Weight [Kg]	7585.54	7147.24	5.77%

Table 4.6: Case study 1: global optimization results.

The results show that a modest reduction of the cost of energy is achieved by the free-form optimization. However, it must be considered that the initial blade

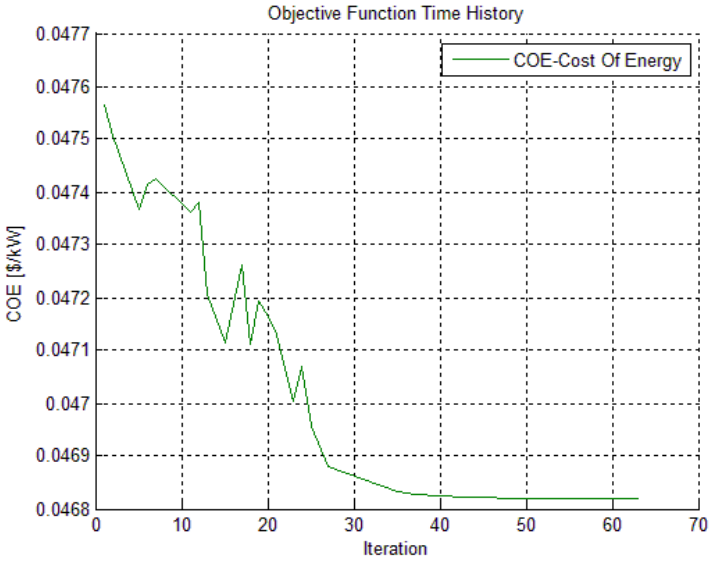

Figure 4.5: Case study 1: time history of the objective function.

configuration is already optimized both aerodinamically and structurally and in this context a reduction of about 1.6% in the cost of energy appears much more significant. Table 4.6 shows that the improvement in the final design was achieved by working simultaneously on the aerodynamic design (to increase AEP) and on the structural design (in order to reduce weight). This is encouraging, since it demonstrates that the free-form algorithm is actually able to manage succesfully the various multi-disciplinary aspects of the blade design. It is also evident that the decrease in the COE was achieved mainly by reducing the weight. This is somewhat expected since the Delft University airfoils used on the initial blade are characterized by a very efficient design, and thus the margin of improvement for what concerns the two-dimensional aerodynamic design is significantly reduced. Table 4.7 illustrates the overall aerodynamic performance of the optimal blade, compared against the initial one.

	Initial	Optimal
C_p^*	0.4758	0.4884
λ^*	7.54	6.84
Ω_{Rated}	15.71 rpm	14.12 rpm
Ω_{Max}	14.88 rpm	14.88 rpm

Table 4.7: Case study 1: aerodynamic performances.

As we can see, the initial power coefficient is already high, due to the use of high-efficiency airfoils on the initial blade. Although this good start point, the free-

	Initial	Optimal
First flapwise frequency [Hz]	0.99	0.8473
3P frequency [Hz]	0.7441	0.7061

Table 4.8: Case study 1: blade frequencies.

form algorithm was able to increase further the aerodynamic behavior, leading the C_p to a significant value of 0.488. It must be noticed that, within a BEM model were tip and hub-loss corrections are employed, this value is close to the highest possible value for this class of machines. An interesting consideration concerns the fact that, having imposed a limit on the tip speed, both the configurations must limit their rotor speed to the value of Ω_{Max}, which assures that the acoustic emissions are maintained within an acceptable level. It is interesting to notice that the initial blade is actually limited by this fact since the Ω_{Rated} is higher than the allowable Ω_{Max}. On the contrary, the optimal blade operates at a lower TSR, with a corresponding lower rotor speed, which lies beneath the limit. It follows that, in the final design, there is no region $2\frac{1}{2}$ and, in turn, all the power production below the rated wind speed is obtained at the best conditions. The regulation strategies in the two cases led to the power curves shown in Figure 4.6, where it is evident the increase in the energy production. This could be appreciated to a higher level of detail looking at the torque and at he rotor speed trajectories, which are illustrated respectively in Figure 4.7 and Figure 4.8.

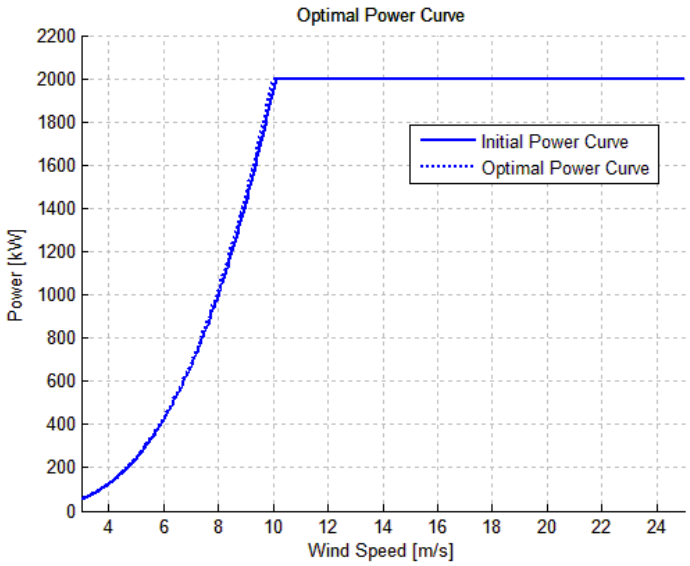

Figure 4.6: Case study 1: power curve

The design of the dynamic behavior of the blade is treated within this work

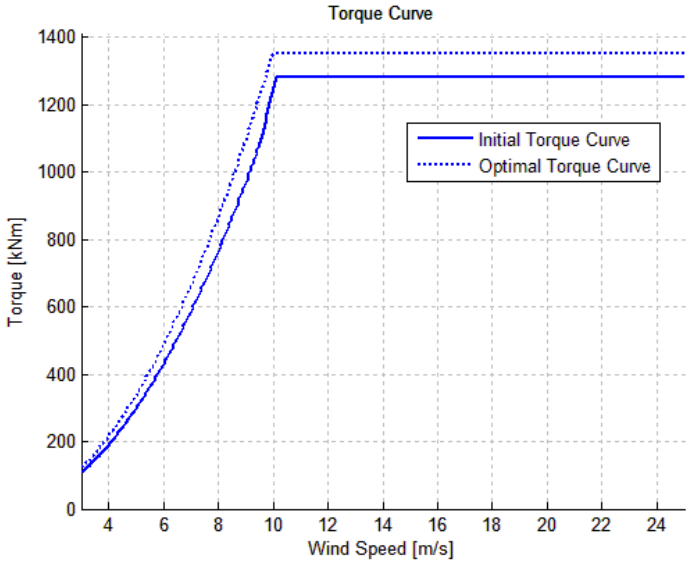

Figure 4.7: Case study 1: torque

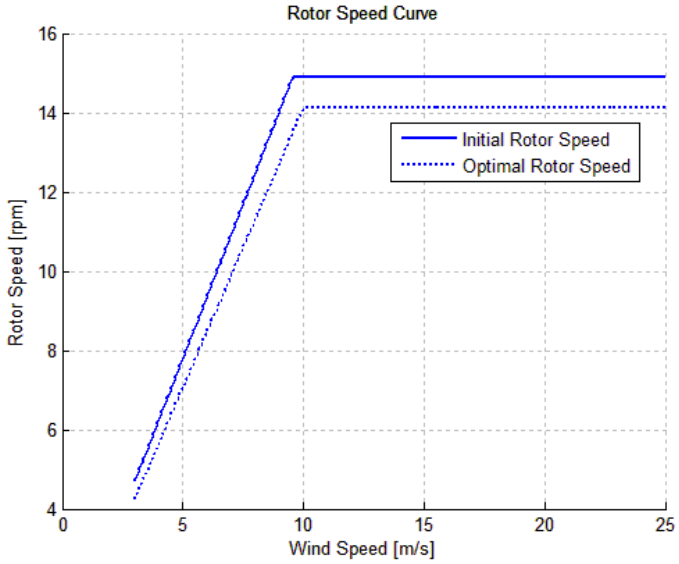

Figure 4.8: Case study 1: rotor speed

by taking into consideration the placement of the first flapwise frequency of the blade, which must be higher than the three-per-revolution (3P) natural frequency up to a required tolerance. The evolution of the dynamic design is summarized in Table 4.8, where the optimal design is compared once again against the intial design. Following our previous considerations, we can appreciate that while the initial value of the 3P is determined by the value of the maximum rotor speed, the final blade shows a lower value of the natural frequency, due to the fact

that the rotor speed is now lower than the required limit. In this case then the improvement in the aerodynamic behaviour led to a less strict structural constraint which, in turn, allows the blade to be more flexible, thus leading to the significant weight reduction experienced in Table 4.6.
After discussing the general performances of the optimal blade, we now concentrate on how the optimization acts on modifying the blade characteristics. The chord and twist functions are reported in Figure 4.9 and Figure 4.10, respectively.

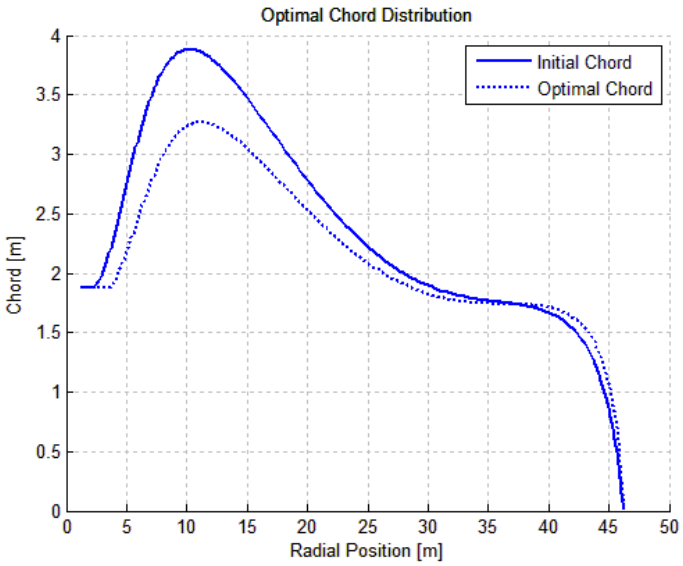

Figure 4.9: Case study 1: chord

The optimal chord distribution led to a lower planform surface of the single blade, that is, a reduced solidity of the rotor. This is a reasonable result, since a smaller chord definitely implies lower weight and a lower complexity of the internal structure, thus leading to a reduced cost of the blade manifacture. On the contrary, it should be pointed out that a blade with a lower solidity should work at an higher TSR, thus leading to an extension of the Region $2\frac{1}{2}$ and to a lower energy production. However, as we discussed above, this is not the case since the optimal blade actually works at a lower TSR than the initial blade. This is a remarkable results of the free-form methodology, and it could be explained by the fact that the reduction of the chord is heavily compensated by increasing the local efficiency of the blade, taht is, by evolving the airfoils towards more efficient shapes. Figure 4.11 shows the local aerodynamic efficiency C_L/C_D along the blade span, while Figure 4.12 presents the local power coefficient at the various locations. As we can see, the local performances are not degraded by the reduced chord but, on the contrary, they are enhanced by the increased local efficiency. It is remarkable to notice that the optimization worked effectively on the power production along the entire blade span, and not only on the typical region of

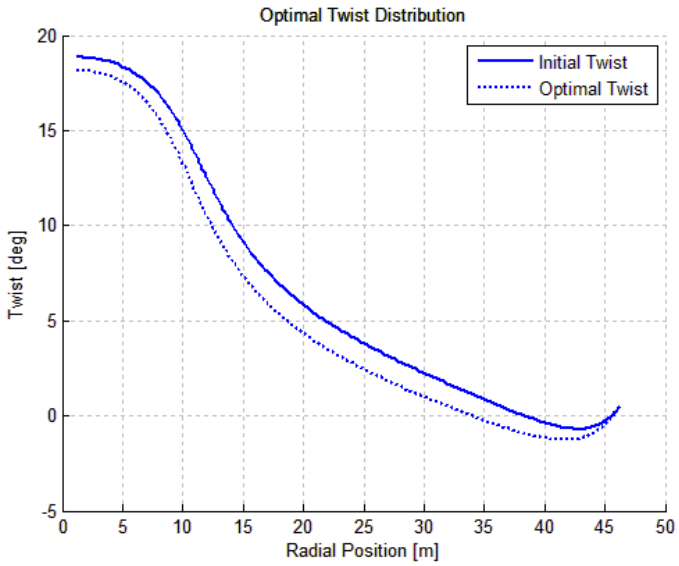

Figure 4.10: Case study 1: twist

production, which typically lies between 0.3R and 0.75R.

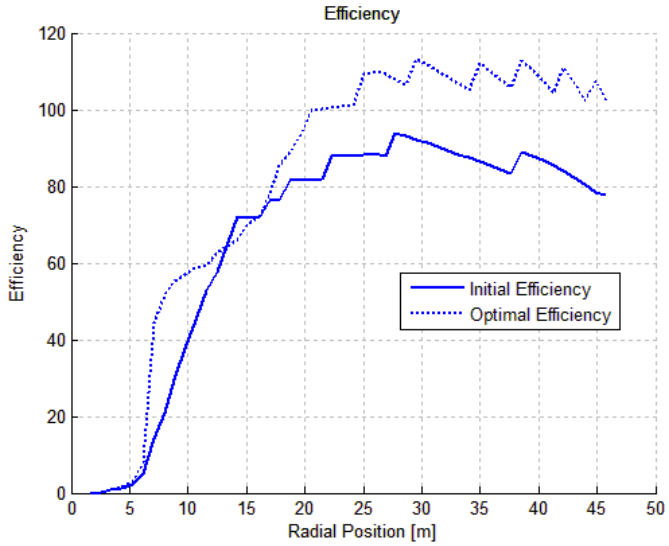

Figure 4.11: Case study 1: local aerodynamic efficiency

The optimal airfoils are illustrated in Figures 4.13 to 4.19. The first figure can refer to both the first and the second cylinders, which are identical and do not change during optimization.
The analysis of the resulting airfoils leads to some interesting consideration. First, it is possible to observe how airfoils placed at different locations along the blade undergo different evolutions. Apart from the cylinders, which are maintained

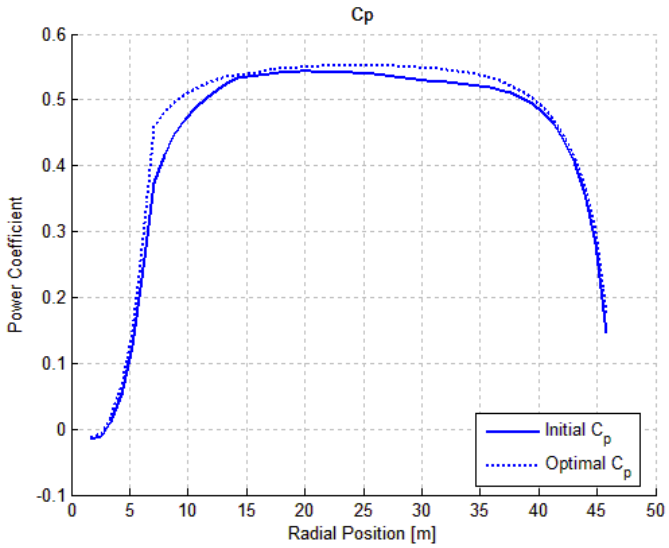

Figure 4.12: Case study 1: local power coefficient

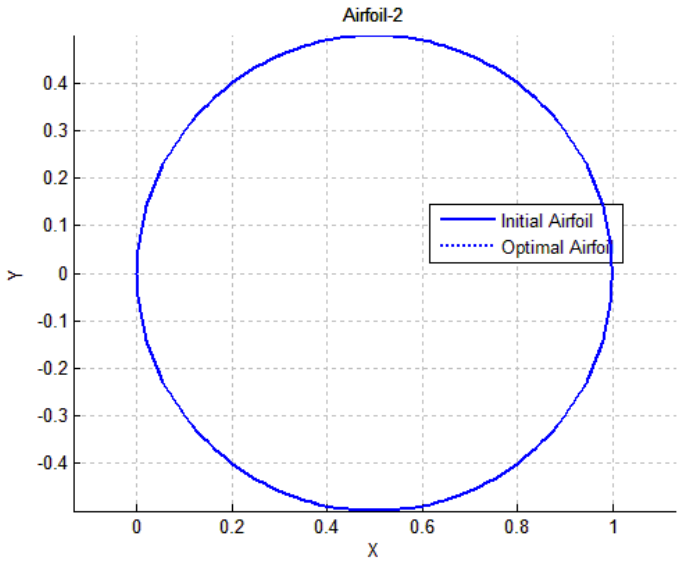

Figure 4.13: Case study 1: airfoil 1,2

in their shapes due to hub connection requirements, the first unfrozen airfoil is the third, which is depicted in Figure 4.14. We can appreciate that the optimization led to a slight reduction of thickness, which was pursued essentially for aerodynamic reasons. In fact, in the region close to the blade root, the presence of thick airfoils result in a significant drag, even if the local velocity is not very high. Then, a reduction of the thickness implies a lower drag and a greater efficiency, which is confirmed also in the plot of Figure 4.11. This reduced thickness

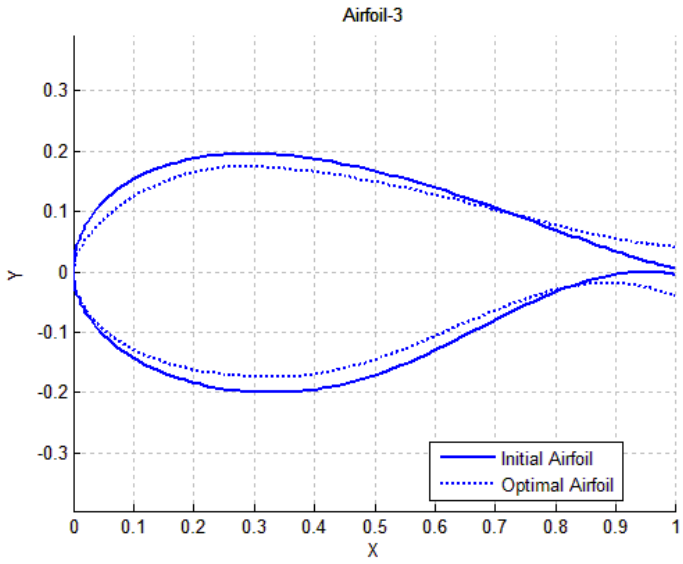

Figure 4.14: Case study 1: airfoil 3

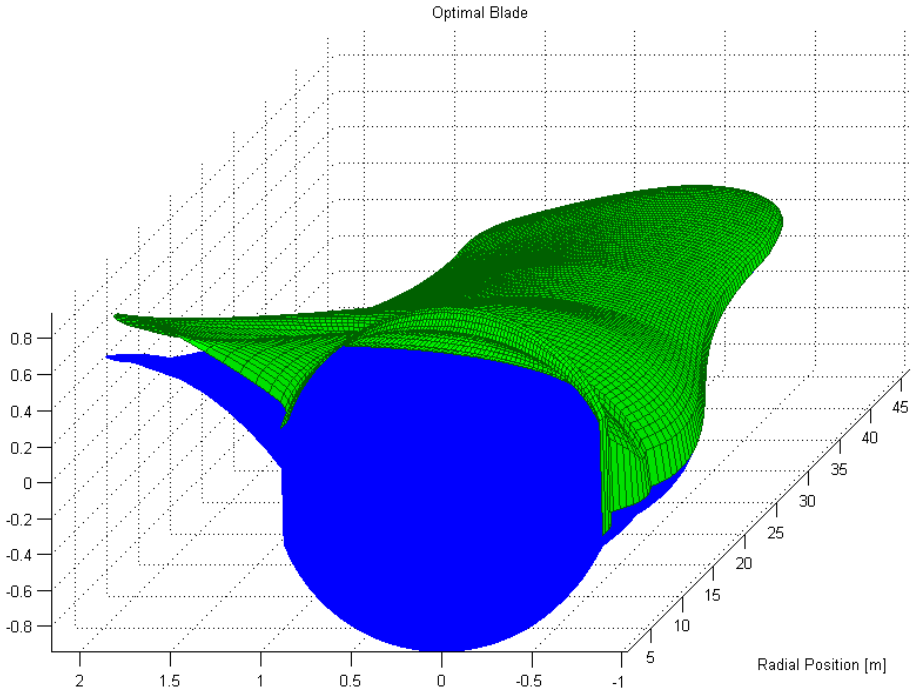

Figure 4.15: Case study 1: 3D view of the optimal blade, which highlights the appearence of flatback airfoils near the hub.

has effects also on the structural behaviour of the blade, since the root region is highly responsible for the bending stiffness. In this view, reducing the sectional thickness could lead to an unacceptable deterioration of the blade stiffness, and it is remarkable to notice that within the optimization this was spontaneously avoided by increasing the trailing edge thickness. This feature can be observed in more detail in Figure 4.15 and the resulting geometry is that of a *flatback airfoil*, which is a common solution adopted in modern wind turbines [28] in order to preserve the useful sectional area without a drastic reduction of the aerodynamic properties of the airfoil. This peculiar characteristics appears, to a lower degree, also in the fourth airfoil of Figure 4.16, where the aerodynamics is also enhanced by an augmentation of the airfoil camber. However, the fact that flatback airfoils emerged naturally from the optimization process represents an encouraging result within the scope of this work.

Looking at the airfoils located in the middle-span region, namely the fifth and the sixth airfoils illustrated in Figure 4.17 and 4.18 we can appreciate how the design drivers migrate from structural to aerodynamic considerations. These airfoils basically experiences minor variations in their thickness, but the geometry is re-arranged in a way that a greater camber magnitude is achieved, thus leading to an increased efficiency. It must be noticed that this region is broadly involved in the energy production, and even a little increase in the local efficiency can affect positively the overall blade performances.

Considering now the tip airfoil, illustrated in Figure 4.19, we notice that the optimization led basically to a reduction of the thickness, in order to limit the drag in a region where the local velocity is maximum, whitout great concern about the generation of more lift. This happens because, considering the massive distance from hub, a great force acting on this airfoil would result in a greater bending moment at root.
The structural design of the blade evolved coherently with the prevoius considerations. Figure 4.20 shows the thickness of the spar caps along the blade: as we can see, the design of the spar cap led to a reduced thickness in the hub region, due to the fact that the smaller chord, together with the increase of stiffness related to the flatback airfoils allows the structural element to be less thick, and this obviously contributes significantly to the overall weight reduction. Towards the tip, on the contrary, we see from Figure 4.9 that the chord is slightly increased, forcing the spar cap to increase the local thickness in order to withstand the stress derived from the introduction of a greater load.
Within the algorithm, the second structural constraints require to verify the stress/strain in the various structural elements under strom conditions. The simulation is done in compliance with international standard, and the results are shown in the following figures. For sake of brevity, only the root flap-wise bending moment is reported, since it plays a direct effect on the sizing of the spar caps:

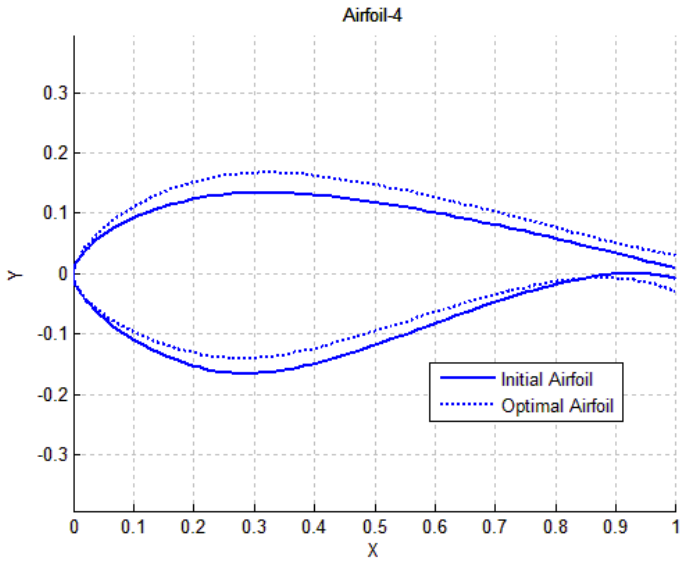

Figure 4.16: Case study 1: airfoil 4

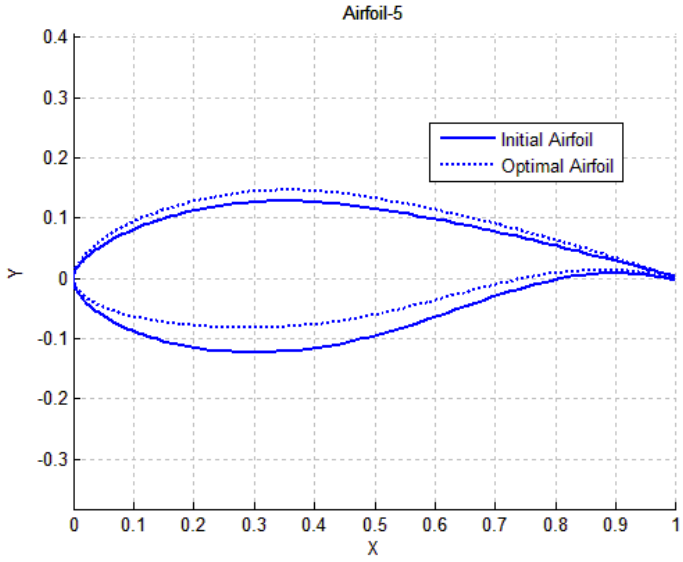

Figure 4.17: Case study 1: airfoil 5

Figure 4.21 shows the reduction in the ultimate bending moment. This derives essentially from the optimal chord, which exhibits globally a smaller planform, assuring that lower loads are introduced in the structure. The corresponding plot of the normal stress acting in the single spar cap is shown in Figure 4.22. Since the stress constraints is everywhere verified, we can conclude that although the optimal blade allows greater stress to take place in the spar cap, due essentially to the reduction of the spar cap thickness, each section is sized correctly in order

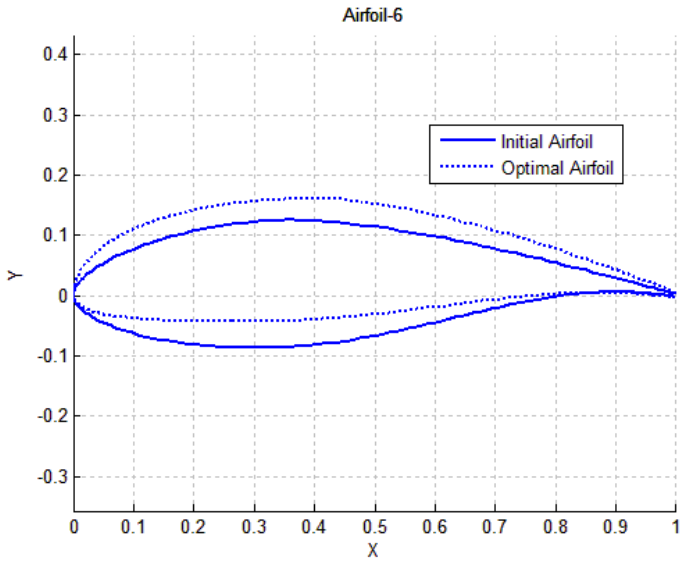

Figure 4.18: Case study 1: airfoil 6

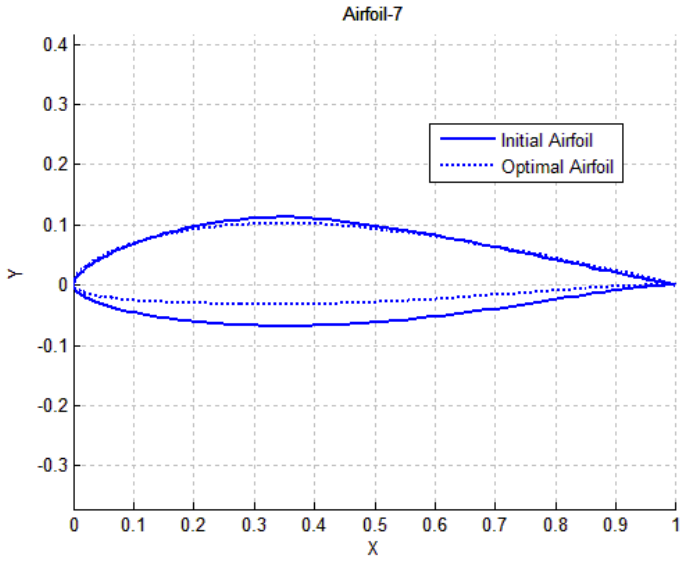

Figure 4.19: Case study 1: airfoil 7

to prevent the stress to reach values too close to the admittable stress.

4.2 DTU-10MW wind turbine

The second case study concerns a large-size wind turbine, which was developed under the Light Weight Rotor project at the Technical University of Denmark,

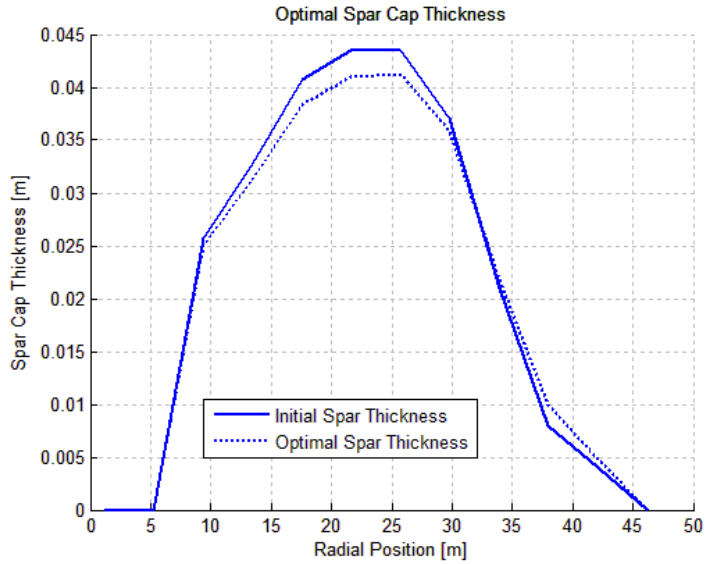

Figure 4.20: Case study 1: spar cap thickness

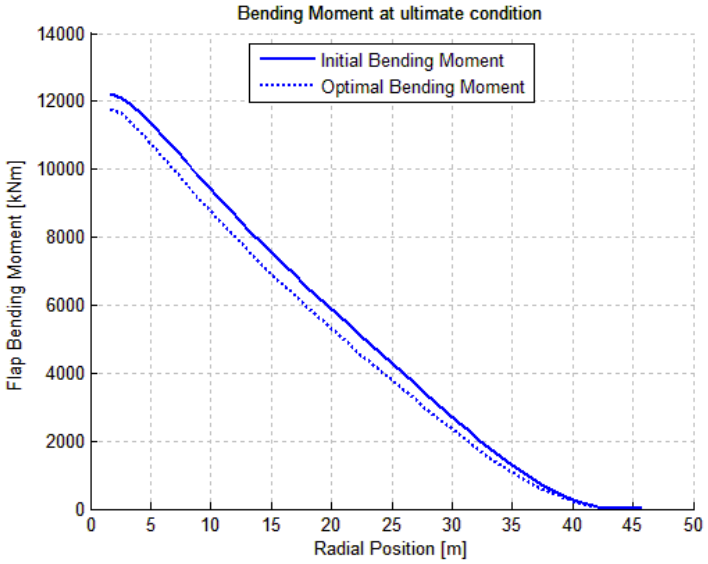

Figure 4.21: Case study 1: root bending moment in storm conditions.

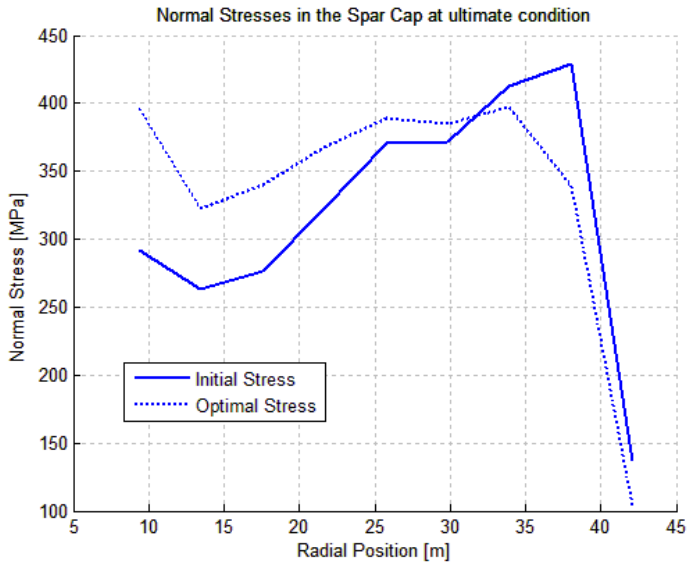

Figure 4.22: Case study 1: spar cap normal stress in storm conditions.

and is currently employed as a reference model within the works of the INNWIND consortium. This machine is characterized by a rated power of 10 megawatts and a rotor size of about 180 meters, and its design was obtained by upscaling a well-known reference machine, specifically the NREL-5MW wind turbine. One of the advantages of working on the DTU-10MW is that all the details of the machine are publicly available and can be freely used for research purposes [29] .

Class	IEC 1A
Rotor orientation	Clockwise, upwind
Control	Variable speed, collective pitch
Cut in speed	4 m/s
Cut out speed	25 m/s
Rated power	10.0 MW
Number of blades	3
Rotor radius	89.17 m
Hub Radius	2.8 m
Cone angle	2.5 deg

Table 4.9: DTU-10MW wind turbine: overall characteristics

The essential overall feature of the machine are reported in Table 4.9, while Figure 4.23 and Figure 4.24 show respectively the planform of the blade and the intial thickness of the structural members.

It must be pointed out that the blade used in this test is actually a simplified

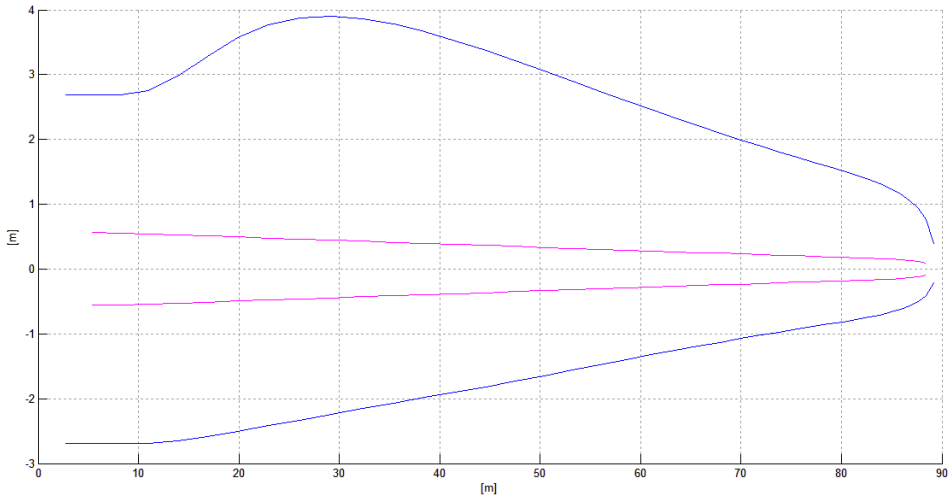

Figure 4.23: DTU-10MW wind turbine: blade planform and spar cap position.

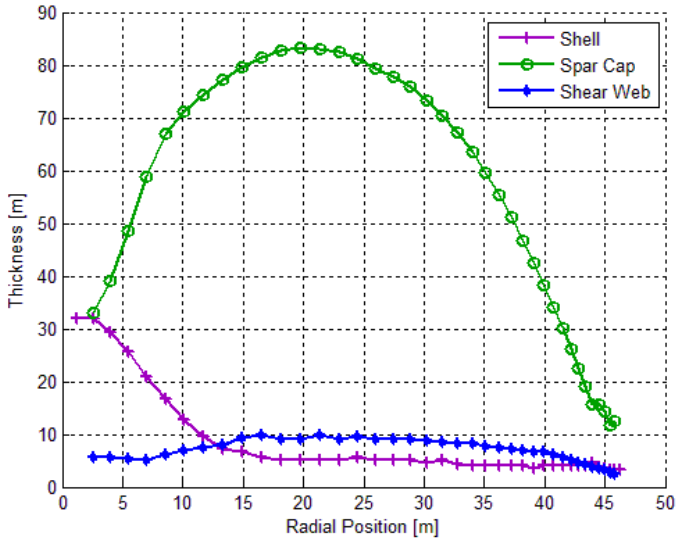

Figure 4.24: DTU-1OMW wind turbine: thickness of the structural elements.

model of the DTU blade. Looking at the detailed description of the structure, which is provided in [29] together with all the relevant data, it is possible to notice that the blade is made up of 11 different layers of materials, which include different materials, fillers and leading edge and trailing edge reinforcements. A detailed transcription of this complex layout within our algorithm would be neither easy to achieve (due to the limit on the number of layers) nor convenient, as a detailed topological description of the section is still not supported by a

complete structural evaluation. Then, the original data were slightly modified in order to obtain a sipler model which, at the same time, maintains the structural features of the DTU blade, specifically the mass distribution, the stiffness and the operating frequencies.

4.2.1 Optimization set-up

Like the first case study, once the initial blade is defined, it is necessary to provide specific informations about the choice of the initial airfoils and the materials. Since all the data regarding the DTU-10MW blade were supposed to be public, the designers choose to equip the blade with airfoils of the FFA-W3-XX series. The geometries of these airfoils are also publicly available, so that a good representation could be achieved, within the free-form algorithm, by the Bézier parameterization, and the resulting airofils are illustrated in Figure 4.25.

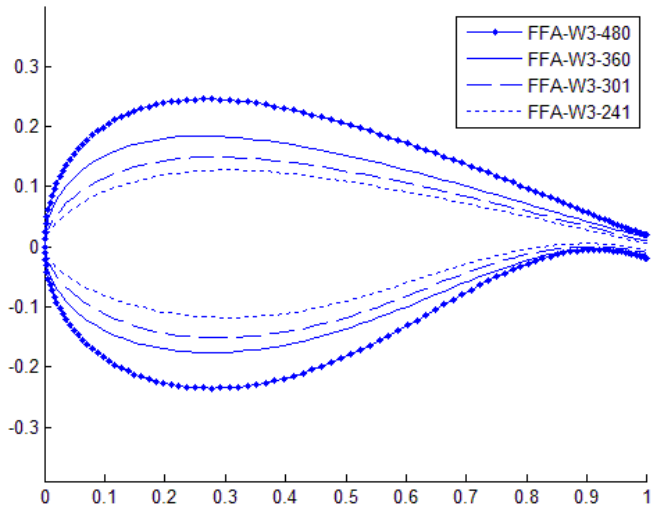

Figure 4.25: FFA-W3-XX airfoil family.

It must be noticed that the DTU-10MW wind turbine is conceived to be relatively light weight. For this reason, the airfoils show a high relative thickness along the entire blade, in order to increase the moment of inertia and thereby increase the stiffness. Within the FFA-W3 series, the airfoil with the maximum thickness is the FFA-W3-360, wich presents a 36 % maximum relative thickness. Since thicker airfoils were needed in the proximity of the hub, the FFA-W3-480 was designed by upscaling the geometry of the FFA-W3-360, in order to obtain a more regular transition between the blade and the cylindrical comnection. For what concerns our simulation, like the previous case study the total number of airfoils along the blade is limited to seven, specifically two frozen and five unfrozen

airfoils. This required to re-arrange the placemement of the airfoils in a way that the relative thickness along the blade is maintained, in order to preserve the structural properties of the original blade. The location of the various airfoils is illustrated in Table 4.25, while Figure 4.26 shows the relative thickness along the blade.

Number	Active	Airfoil	Thickness %	Position $[m]$
1	No	Cylinder	100	2.8
2	No	Cylinder	100	8.0
3	Yes	FFA-W3-480	48	21.0
4	Yes	FFA-W3-360	36	28.5
5	Yes	FFA-W3-301	30	36.0
6	Yes	FFA-W3-241	24	50.0
7	Yes	FFA-W3-241	24	89.17

Table 4.10: DTU-1OMW wind turbine: Initial airfoils distribution.

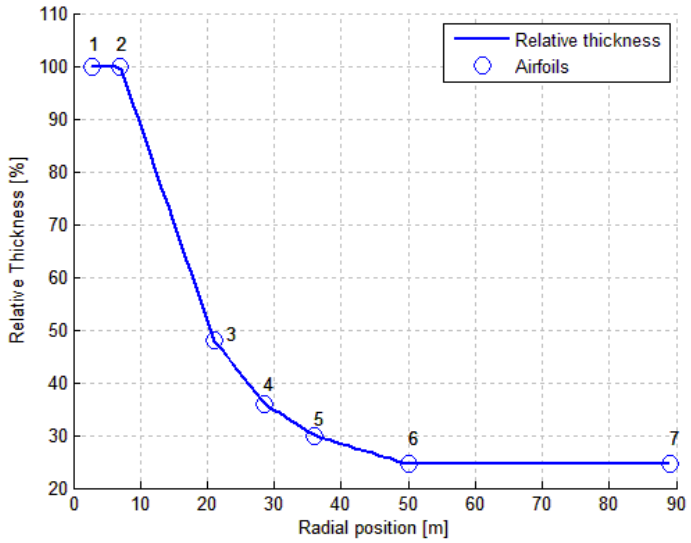

Figure 4.26: DTU-1OMW wind turbine: relative thickness.

The derivation of the material properties was performed, like in the previous case study, by means of the classic lamination theory. This allowed to derive the mechanical properties of the multi-directional plys illustrated in Table 4.11.

Material	Element	E_x	E_y	G	ν_{xy}	ρ	$\sigma_{x\ max}$
		[MPa]	[MPa]	[MPa]		[Kg/m^3]	[MPa]
Triaxial	Shell	21790	14670	9413	0.478	1845	392
Biaxial	Webs	13920	13920	11500	0.533	1845	208
Uniaxial	Spar Caps	41630	14930	5047	0.241	1915	624

Table 4.11: DTU-1OMW wind turbine: Materials.

4.2.2 Results

The second case study was run under the same conditions of the previous example, and the overall performances of the free-form algorithm are summarized in Table 4.12.

Total computational time	66.36 hours
Total number of iterates	72
Covergence tolerance	1.0e-8
Value of Frequency constraint at convergence	-5.51e-03
Value of Stress constraint at convergence	-2.28e-06

Table 4.12: Case study 2: algorithm performances.

Again, the total computational time is in the order of days, and comparable against the previous case study. The value of the constraints, on the contrary, show that the design of the DTU-10MW rotor blade was driven essentially by considerations of ultimate stress, and this is demonstrated by the final value of the stress constraint, which is much smaller than the corresponding frequency constraint. Table 4.13 shows the total variation of the main parameters, specifically the cost of energy, the AEP and the blade mass between the intial and the final solutions.

	Initial	Optimal	Gain
Cost of energy [$/kWh]	0.112346293	0.111197805	1.022%
Annual Energy Production [kWh/yr]	3.4182e07	3.4554e07	1.0891%
Blade Mass [Kg]	41067.10	40194.63	2.12%

Table 4.13: Case study 2: global optimization results.

Again, it can be appreciated how the optimization affects both the aerodynamic design and the structural design in order to minimize the cost of energy. However, the relative reduction of the cost is smaller than the one obtained for the 45-meters blade, and this suggests that the initial blade is designed to be very close

to the actual optimal point. Nevertheless, the saving of about 1 % cost confirms the capability of the free-form methodology to push the design towards better configurations. The time-history of the objective function (cost of energy) is depicted in Figure 4.27, which highlights the typical plateau of convergence of the optimal solution.

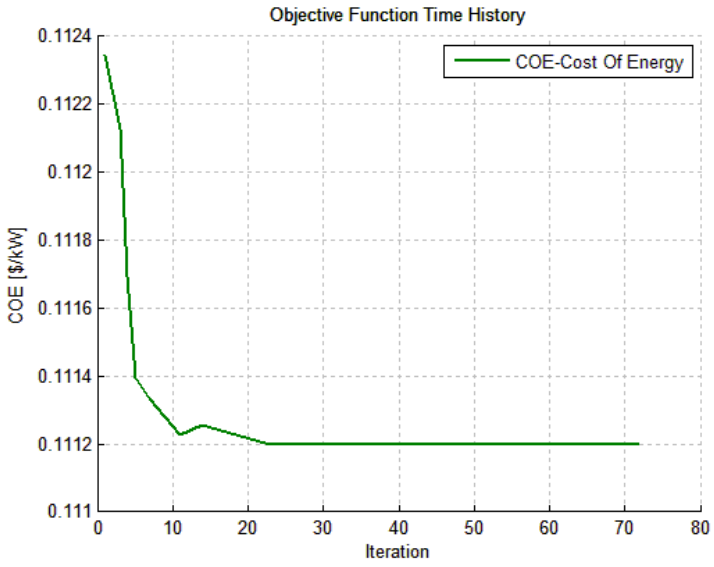

Figure 4.27: Case study 2: time history of the objective function.

The results of the aerodynamic design are summarized in Table 4.14. It is important to notice how the significant size of the rotor makes the DTU-10MW wind turbine to work at lower rpm than the previous 2MW blade, which corresponds to a greater flexibility of the blade. We can notice also that onshore operating conditions are simulated and a tip-speed constraint is imposed, so that the maximum rotor speed is bounded by the value of Ω_{Max}. As discussed above, this means that the computation of the regulation trajectories is affected by the presence of a region $2\frac{1}{2}$ where the aerodynamic behaviour of the blade departs from the optimal $[C_P^*, \lambda^*]$ conditions.

	Initial	Optimal
C_p^*	0.4750	0.4843
λ^*	7.3317	7.19
Ω_{Rated}	8.73 rpm	8.51 rpm
Ω_{Max}	7.71 rpm	7.71 rpm

Table 4.14: Case study 2: aerodynamic performances.

The evolution of the design led to an increased value of the power coefficient, to-

gether with a reduction of the nominal rotor speed. These factor both contribute to the increase in the energy production since, first, a better power coefficient assures a greater production below the power rated and, second, the reduced rotor speed implies a reduced extension of the region $2\frac{1}{2}$. From this point of view, the results are consistent with the results obtained in the 2MW case study. As outlined before, the nominal rotor speed has implications in the dynamic design of the blade, as it drives the three-per-revolution natural frequency. Table 4.15 shows the intial and optimal frequencies of the blade, specifically the first flapwsie frequency and the 3P.

	Initial	Optimal
First flapwise frequency [Hz]	0.6466	0.6750
3P frequency [Hz]	0.3855	0.3855

Table 4.15: Case study 2: blade frequencies.

As we observed before, in this case the optimal desing is not determined by frequency considerations. Looking at the table, the first flap-wise frequency is increased, while the 3P remains the same, since it is determined by the maximum rotor speed. The consequence is that the optimal design makes the blade more stiff (at least in the flap-wise direction) and a greater clearance between the first flap-wise frequency and the 3P is obtained. Figures 4.28 to 4.30 illustrate the regulation trajectories, specifically the power curve, the torque and the rotor speed. It must be noticed that the differences in the initial and final designs are minimal, and they coud not be fully appreciated from the power curve.
The external design of the final blade is illustrated in Figure 4.31 and Figure 4.32. While the twist seems to experience minor variations, the chord function is definittely changed. It is interesting that, in this case, the chord is increased near the hub. This leads to an increased flapwise stiffness and, consequently, to the higher frequency of the blade.
The combined 2D/3D aerodynamic design led to a global increase in the aerodynamic performances along the blade. The results can be appreciated in Figure 4.33, where the local aerodynamic efficiency is shown, and in Figure 4.34 which shows the local power coefficient. It is remarkable to notice that a significant variation of the local properties has been achieved in the hub-region of the blade. This can be seen especially in the power coefficent curve, which results to be heavily increased in this region. As the overall design is limited by the ultimate normal stress in the structural elements, a natural consequence is that the optimization acts more sharply in those area, specifically the hub region, where the value of the stress is more distant from the maximum admittable stress.
The design of the airfoils evolved coherently with the blade. In the following, three of the five active airfoils are reported, and their optimal shapes are illustrated in

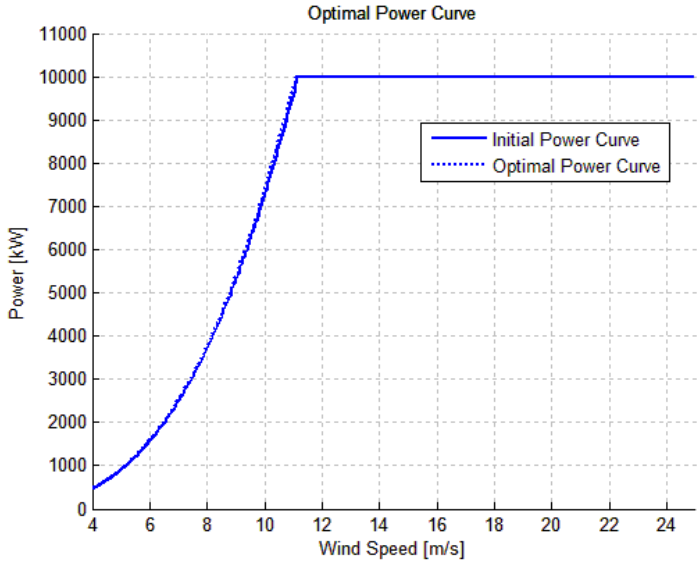

Figure 4.28: Case study 2: power curve

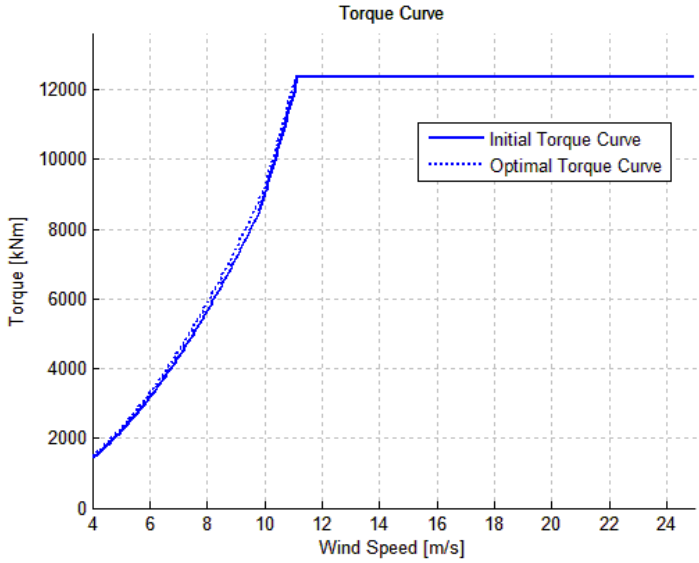

Figure 4.29: Case study 2: torque

Figures 4.35 to 4.37. It is remarkable to notice that the airfoil 3, which is the first active airfoil along the blade, followed a design strategies similar to that obtained in the 2MW rotor blade example. Again, the final design is that of a flatback airfoil, in which the reduction of the sectional area due to the reduced thickness is compensated by an increased thickness at the trailing edge.
An additional observation regards the desing of the middle-span airfoils, like the fifth airfoil of Figure 4.36. We can notice that the increase in the local efficiency

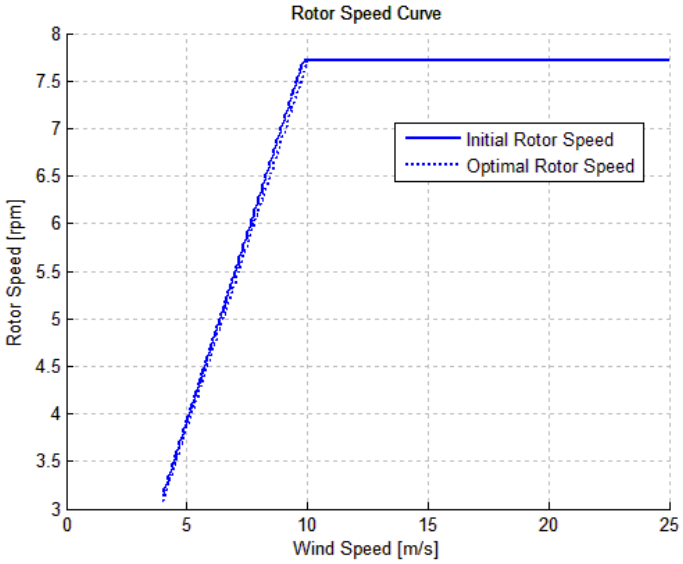

Figure 4.30: Case study 2: rotor speed

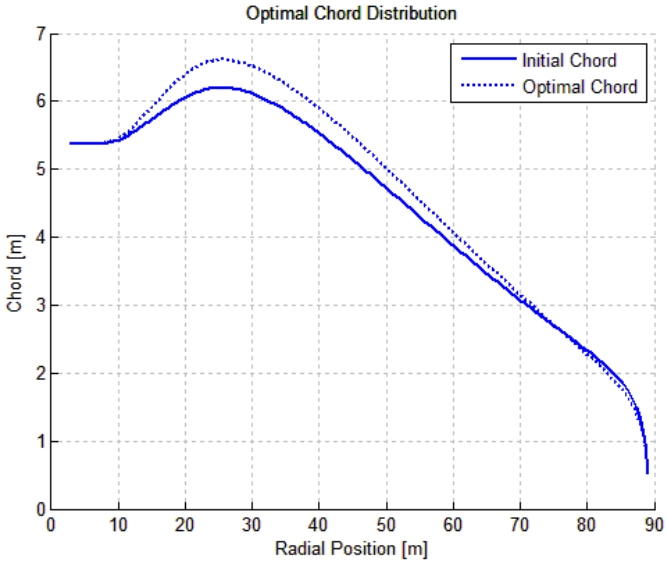

Figure 4.31: Case study 2: chord

was achieved mainly by reducing the thickness, in order to reduce drag, rather than increasing the camber. This is again related to the fact that the blade design is heavily affected by the normal stress. In this context, even a slight increase of the airfoil camber would result in a significant increase in the aerodynamic loads and, consequently, the local value of the stress. This behaviour can be observed also in the tip-airfoil, specifically the airfoil 7 of Figure 4.37. Here, the thickness is reduced asymmetrically, which implies that the camber is modifed too, but we

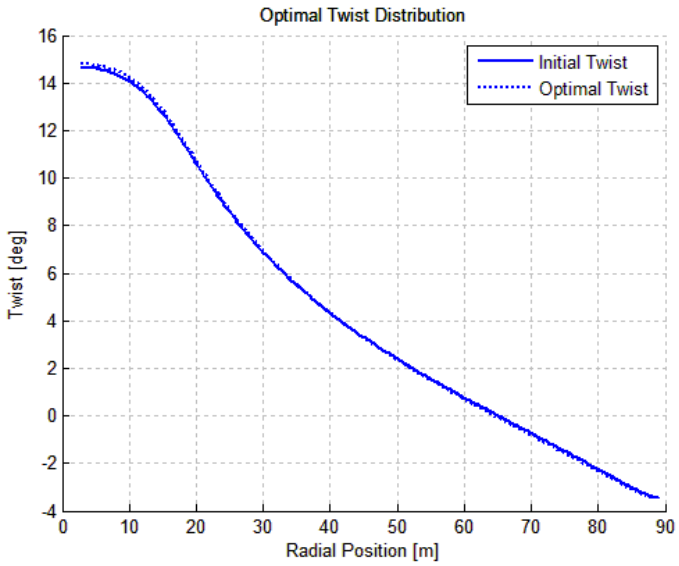

Figure 4.32: Case study 2: twist

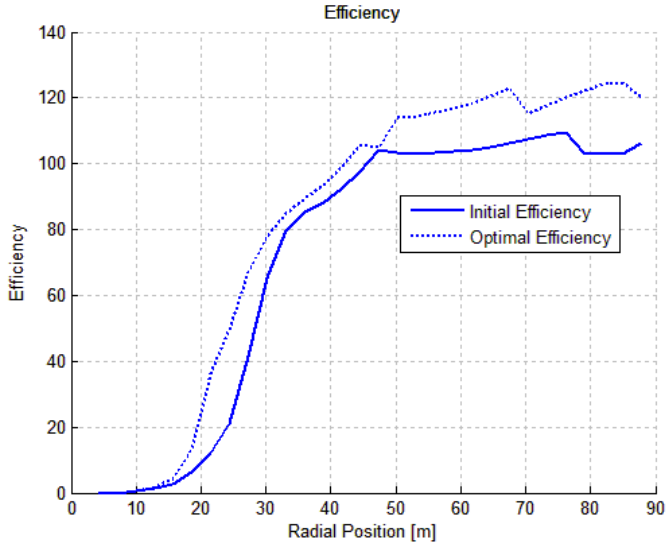

Figure 4.33: Case study 2: local aerodynamic efficiency

must notice that in the tip region the chord planfomr is slightly reduced, so that the increase in the local stress due to the higher camber is compensated by the reduction of the local chord.

The evolution of the structural design is summarized by the optimal spar cap thickness, which is reported in Figure 4.38. Here we can notice that the area where the highest reduction is achieved is near the hub. In fact, while the local thickness of the airfoils is generally lower, the increase in the local chord and the

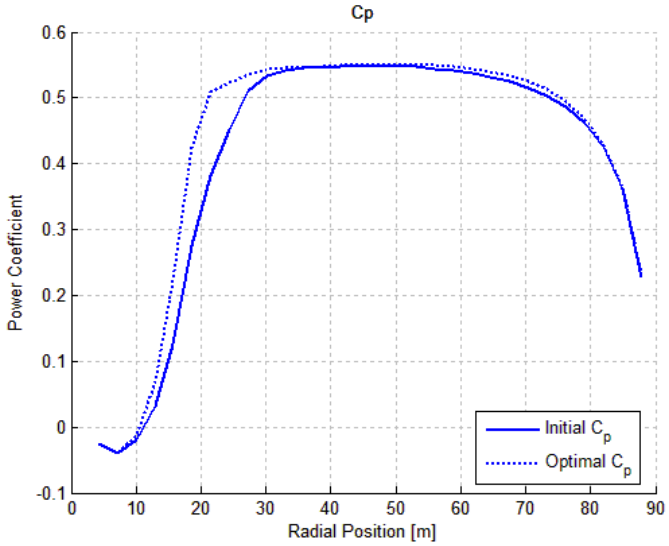

Figure 4.34: Case study 2: local power coefficient

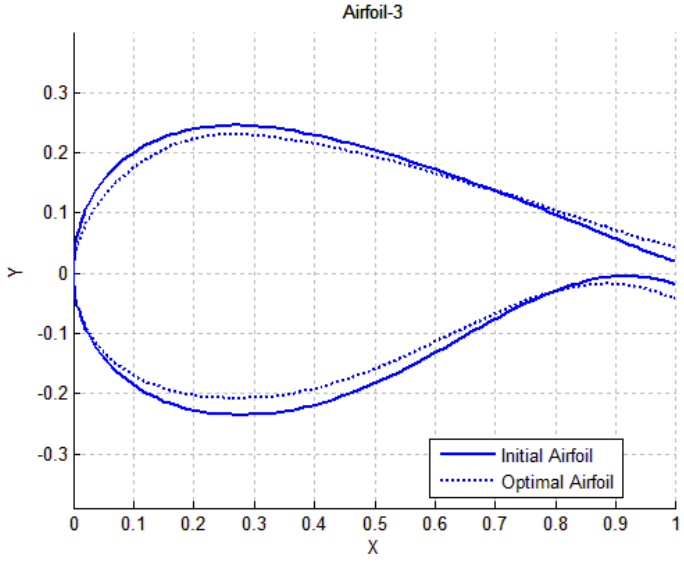

Figure 4.35: Case study 2: airfoil 3

appearence of flatback airfoils guarantee that a useful sectional area is preserved. The resulting flapwise bending moment at root in storm conditions is illustrated in Figure 4.39. The increased aerodynamic properties, together with a larger blade surface generate a higher bending moment, which results in the optimal stress distribution depicted in Figure 4.40. It is important to notice that, globally, the value of the local stress is increased everywere, and the highest value is obtained at about $R = 60m$, in the middle of the power-generation area.

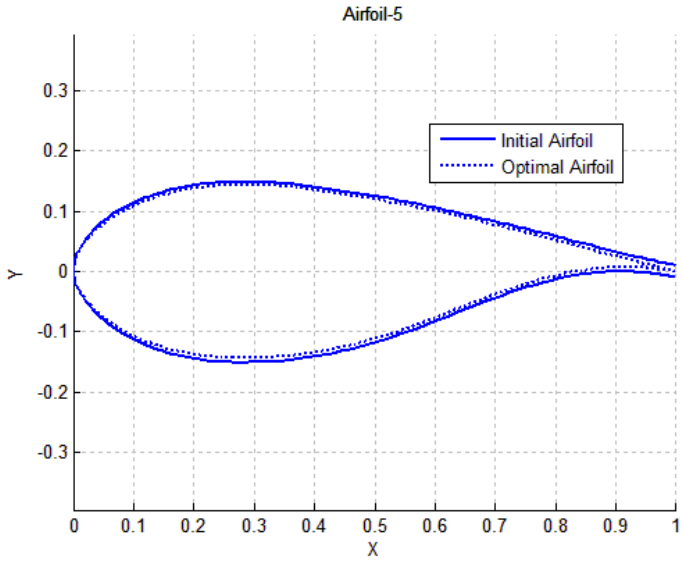

Figure 4.36: Case study 2: airfoil 5

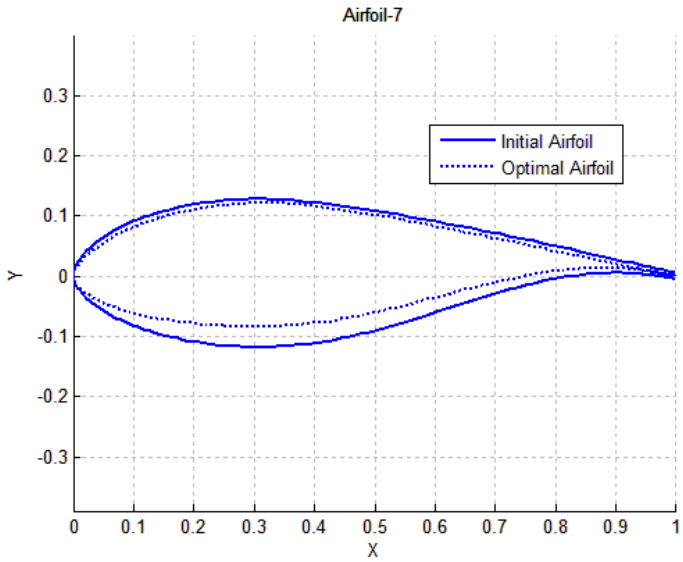

Figure 4.37: Case study 2: airfoil 7

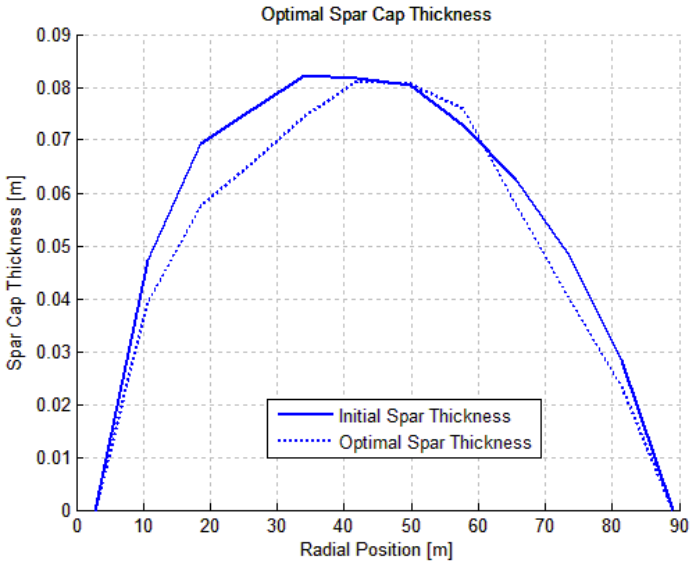

Figure 4.38: Case study 2: spar cap thickness

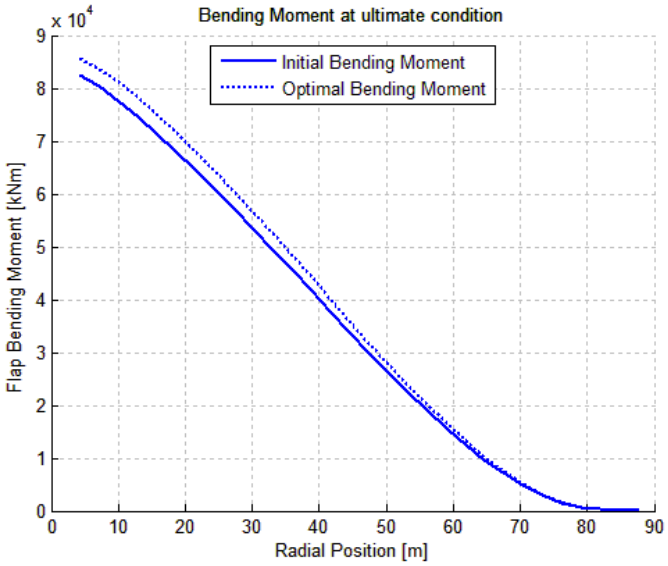

Figure 4.39: Case study 2: root bending moment in storm conditions.

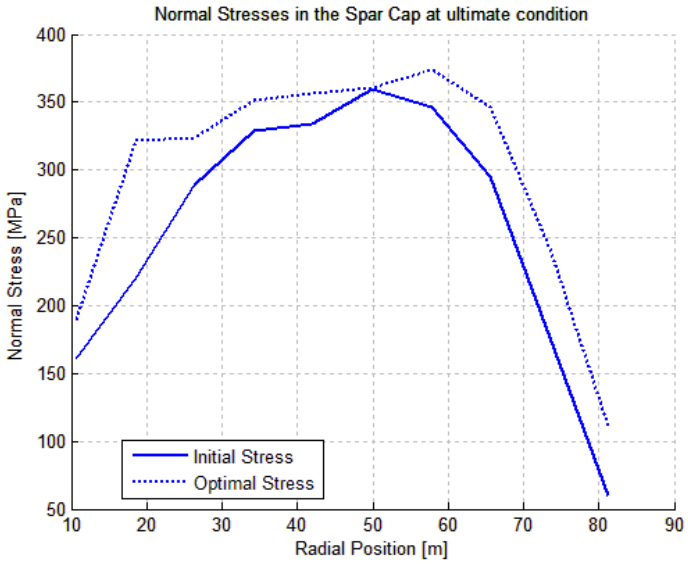

Figure 4.40: Case study 2: spar cap normal stress in storm conditions.

Chapter 5

Conclusions

This work explored a common limitations of the traditional numerical algorithms employed for rotor blades optimization. It was discussed how the use of BEM models or lifting line models for the description of the three-dimensional aerodynamic behaviour of the blade relies on User-provided data concerning the properties of the various airfoils, which are considered as a forcing term during the entire optimization process. To overcome this limit, an improvement of the current methodolgy based on a free-form approach has been investigated, in order to understand if the inclusion of the airfoil geometries within the optimization process can lead to an improved ability to meet the design requirements. In order to enforce this study, a new algorithm for the aero-structural optimization of wind turbine blades has been developed, following a multi-disciplinary approach so that all the relevant aspects of the design can be taken into consideration. The algorithm relies on an interative procedure which solves cyclically several sub-problems, in order to define the blade properties in terms of aerodynamics, structural sizing and dynamic response. The evolution of the design takes place within a searchable domain which is bounded by several non-linear constraints, which are imposed in compliance with international standard. The algorithm was then tested on two reference machines of the multi-megawatt class.
The analysis of the results allows to draw some conclusions about the functioning and the convenience of the free-form methodology. A first set of observations can be made about the general behaviour of the program and, in particular:

- The algorithm appears to be able to represent real-world rotor blades to a high degree of accuracy. Specifically, the parameterization based on the Bézier curve assures that the blade shape and the geometries of the airfoils are reproduced with great confidence.

- A typical optimization cycle shows a time-to-convergence in the order of several days on a normal laptop, which is comparable against traditional rotor blade optimization algorithms. The increased computational time

ascribable to the presence of unfrozen airfoils is compensated by the intrinsic simplicity of the models.

- The algorithm is able to manage succesfully all the different families of design variables, without incurring in bad-conditioning problems. This was a crucial aspect of the code development and a lot of time was dedicated to make the optimization coherent and harmonical through all the design variables.

For what relates to the specifical aspects of the free-form methodolgy, it is possible to draw the following conclusions:

- The program works effectively even if the initial blade shows very good performances. We conclude that the ability to adapt the airfoils to the local requirements as they change during the optimization can lead to a better design.

- The optimal design of the various airfoils pursues different goals depending on the position of the airfoil along the blade. Specifically, the airfoils close to the hub region are driven by structural and stiffness considerations, while moving towards the tip implies a greater role of the arodynamic design. This behavior, which is actually typical of rotor blade design, was achieved by means of only general constraints, i.e. no requirements about local camber and thickness were applied.

- Some typical solutions adopted in large wind turbines emerged naturally during the design of the airfoils, like for example the presence of flatback airfoils near the hub and the appearence of typical S-tail in the lower surface.

Globally, we can conclude that the objectives of this work have been met. The free-form methodology seems to provide an improved ability to meet the design requirements and, moreover, it allows the designer to be less specific for what concerns the design of the initial airfoils. As the airfoils are automatically tailored to meet the features of the optimal blade, the onerous task of forecasting in advance the local properties of the airfoils can be moved from the designer to the optimization algorithm, provided that physical-meaningful constraints are imposed on the final design.

5.1 Future developments

This work was conceived to be a preliminary study of the free-form methodology, and thus it shows some intrinsic limitations which must be addressed and possibly corrected in further, more deepened, investigations. Some ideas for future developments of this work are here proposed:

- In this first version of the program, the numerical estimation of the airfoil characteristics is done by `XFOIL`. It was noticed, however, than this solver limits its effectiveness to the pre-stall region. While this was not actually a problem within our simple analysis, a greater effectiveness of the airfoil design could be achieved by a better description of the near-stall and the post-stall regions. ECN devloped for this purpose `RFOIL`, which is a refined version of `XFOIL` with a more accurate description of the airfoil behaviour at higher angles of attacks. An example of its application in airfoil design is provided by Grasso in [11] and [12]. A possible alternative solutions could be to replace a panel-method solver with a 2D finite element solver, in which the Naviér-Stokes equation are solved directly. An example of this approach was pursued by Dahl and Fuglsang for the development of the `EllipSys2D` solver [30], but its convenience within large optimization algorithms should be evaluated carefully.

- The set of the structural design variables in this analysis includes only the thickness of the spar cap along the blade. A refined version of the program should allow a broader level of freedom of the structural design, through the introduction of additionl degrees of freedom associated with the other structural elements, specifically the shell and the shear webs. This could be achieved easily by minor modifications of the structural modules within the program and, obviously, one or more new constraints should be added in order to take into account the phenomena which affect these structural elements, like for example a buckling verification.

- It must be noticed that, so far, no specifical requirements on the airfoil shapes have been used. This means that the airfoils evolve only under the action of the two global structural constraints. In real world, however, the design of wind turbine dedicated airfoils is also affected by 2D considerations, for example by imposing limits on the maximum lift coefficient, or by prescribing the behaviour of the boundary layer at certain angles of attack. It would be interesting to introduce such constraints in the algorithm, to verify how the optimal design changes.

- The use of `WT Perf` as BEM solver was decided for sake of simplicity. Although it proved to be fast and reliable it only supports elementary, turbulence-free scenarios. There are more sophisticated softwares which could be used in order to grant a more detailed description of the wind field, for example the popular `AeroDyn`, which is generally coupled with `TurbSim` for the simulation of turbulent conditions. It would be very interesting to improve the program with these modules but, in this case, a more detailed description of the airfoil stall must be assured, in order to allow the use of the Beddoe's dynamic stall models included in `AeroDyn` [31].

- It would be interesting, also, to test the free-form methodolgy within a high-complexity optimization algorithm, with full support of the DLCs and full dynamic simulation. This kind of analysis could rely on the `Cp-Max` solver developed at Politecnico, and would allow to study the impact of the free-form airfoil design on fatigue and Actuator Duty Cycles under all the conditions required by international certification guidelines.

- Since a gradient-base optimization method is employed, the dependencies on the initial condition should be evaluated carefully. At present, a paramteric analysis is running in order to estimate the ability of the program to obtain unique optimal solutions for different intial conditions, and the results will be presented at the next EWEA conference in Barcelona, on March 2014. If a strong dependency on the initial blade will be demonstrated, a possible countermeasure should be to introduce a hybrid approach, based on the coupling between a global optimization algorithm with the SQP employed in this study. This should bring to a greater robustness of the program.

Bibliography

[1] E. T. G. Bot and O. Ceyhan. *Blade Optimisation Tool User's manual*. ECN-E–09-092. 2011. URL: http://www.ecn.nl/docs/library/report/2009/e09092.pdf.

[2] C.L. Bottasso, F. Campagnolo, and A. Croce. *Computational Procedures for the Multi-Disciplinary Constrained Optimization of Wind Turbines*. DIASR 10-02. Dipartimento di Ingegneria Aerospaziale, Politecnico di Milano, Milano, Italy, 2010.

[3] M. Drela. "Pros and Cons of Airfoil Optimization". In: *Frontiers of Computational Fluid Dynamics* (1998).

[4] G. Venter. "Review of Optimization Techniques". In: *Encyclopedia of Aerospace Engineering* (2010). Ed. by John Wiley and Sons.

[5] J.L. Zhou, A.L. Tits, and C.T. Lawrence. *User's guide for FFSQP version 3.7: A fortran code for solving optimization programs, possibly minimax, with general inequality constraints and linear equality constraints, generating feasible iterates*. 1997.

[6] Paul T. Boggs and Jon W. Tolle. *Sequential Quadratic Programming*. 1995.

[7] L. Fingersh, M. Hand, and A. Laxson. *Wind Turbine Design cost and Scaling Model*. NREL/TP-500-40566. Golden, Colorado, USA, 2006.

[8] Anonymus. *Wind Turbines Part 1: Design Requirements*. International Standard IEC 61400-1. 2005.

[9] Germanischer Lloyd. *Guideline for the Certification of Wind Turbines*. Hamburg, Germany, 2010.

[10] A.L. Rogers and J.F. Manwell. *Wind Turbine Acoustic Noise*. Golden, Colorado, USA, 2002.

[11] Francesco Grasso. "Development of Thick Airfoils for wind Turbines". In: *50th AIAA Aerospace Sciences Meeting*. Vol. AIAA 2012. Nashville, TN, USA, 2012, p. 0236.

[12] Francesco Grasso. "Design and Optimization of Tidal turbine airfoil". In: *29th AIAA Applied Aerodynamics Conference*. Vol. AIAA 2011. Honolulu, HI, USA, 2011, p. 3816.

[13] R. Mukesh, K. Lingadurai, and A. Muruganandham. "Application of PARSEC Geometry Representation to General Airfoil for Aerodynamic Optimization". In: *Lecture Notes in Information Technology* 10 (2012), pp. 55–60.

[14] M. Drela. *XFOIL 6.94 User Guide*. 2001.

[15] L.A. Viterna and R.D. Corrigan. "Fixed pitch rotor performance of large horizontal axis wind turbines". In: *DOE/NASA Workshop on large horizontal axis wind turbines*. Cleveland, Ohio, USA, 1981.

[16] Francesco Grasso. "Usage of Numerical Optimization in Wind Turbine Airfoil Design". In: *28th AIAA Applied Aerodynamics Conference*. Chicago, IL, USA, 2010.

[17] Ira H. A. Abbott. *Theory of Wing Sections: Including a Summary of Airfoil Data*. New York: Courier Dover, 1959.

[18] Morten Hartvig Hansen. "Aeroelastic instability problems for wind turbines". In: *Wind Energy* 10.6 (2007), pp. 551–577. ISSN: 1095-4244.

[19] A. D. Platt and M. L. Buhl. *WT Perf User Guide for Version 3.05.00*. Golden, Colorado, USA, 2012.

[20] Tony Burton et al. *Wind Energy Handbook*. Wiley, 2011.

[21] C.L. Bottasso et al. *Structural Optimization of Wind Turbine Rotor Blades by Multi-Level Sectional/Multibody/3DFEM Analysis*. DIA-SR 12-01. Dipartimento di Ingegneria Aerospaziale, Politecnico di Milano, Milano, Italy, 2012.

[22] G. Bir. *User's guide to BModes (Software for computing rotating beam coupled modes*. NREL/TP-500-39133. National Renewable Energy Laboratory, Golden,Colorado, 2005.

[23] J.P. Blasques and R. Bitsch. *User's Manual for BECAS - a cross section analysis tool for anisotropic and inho-mogeneous beam sections of arbitrary geometry*. DTU, Roskilde, Denmark, 2012.

[24] G. L. Ghiringhelli and P. Mantegazza. "Linear, straight and untwisted anisotropic beam section properties from solid finite elements". In: *Composites Eng* 4.12 (1994), pp. 1225–1239.

[25] V. Giavotto, M. Borri, et al. "Anisotropic Beam Theory and Applications". In: *Computers and Structures* 16.1-4 (1983), pp. 403–413.

[26] Franck Bertagnolio et al. *Wind Turbine Airfoil Catalogue*. Roskilde, Denmark: Risø National Laboratory, 2001.

[27] C. Chamis. *Simpified composite cicromechanics equations for hygral, thermal and mechanical properites*. NASA Technical Memorandum 83320. Lewis Research cCenter, Cleveland, Ohio, 1983.

[28] J.A. Paquette and P.S. Veers. "Increased Strength in Wind Turbine Blades through Innovative Structural Design". In: *European Wind Energy Conference and Exhibition*. Milan, Italy, 2007.

[29] C. et al. Bak. *Description of the DTU 10 MW Reference wind turbine*. DTU Wind Energy Report-I-0092. 2013.

[30] K.S. Dahl and P. Fuglsang. *Design of the wind turbine airfoil family Risø-A-XX*. Risø-R-1024(EN). 1998.

[31] P.J. Moriarty and A.C. Hansen. *AeoDyn theory manual*. NREL/TP-500-36881. 2005.

[32] Andrew Ning, Rick Damiani, and Patrick Moriarty. "Objectives and Constraints for Wind Turbine Optimization". In: *51st AIAA Aerospace Sciences Meeting including the New Horizons Forum and Aerospace Exposition*. Grapevine, Texas, USA, 2013.

[33] Jin Chen et al. "Optimization design of blade shapes for wind turbines". In: *Jixie Gongcheng Xuebao* 46.3 (2010), pp. 131–134. ISSN: 0577-6686.

[34] Danny Sale. *HARP-Opt User's Guide*. 2010.

[35] Kevin Maki, Ricardo Sbragio, and Nickolas Vlahopoulos. "System design of a wind turbine using a multi-level optimization approach". In: *Renewable Energy* 43 (2012), pp. 101–110.

[36] Fujio Yamaguchi. *Curves and surfaces in computer aided geometric design*. Springer, 1988, pp. I–X, 1–378. ISBN: 978-0-387-17449-5.

[37] Gustave P. Corten. *Flow Separation on Wind Turbine Blades*. Utrecht, The Netherlands: Proefschrift Universiteit Utrecht, 2001.

[38] J. Fazil and V. Jayakumar. "Investigation of airfoil profile Design Using Reverse Engineering Bezier Curve". In: *ARPN Journal of Engineering and Applied Sciences* 6.7 (2011).

[39] J. Jonkman et al. *Definition of a 5-MW Reference Wind Turbine for Offshore System Development*. NREL/TP-500-38060. Golden, Colorado, USA, 2009.

[40] M. Jureczko, M. Pawlak, and A. Mezyk. "Optimisation of wind turbine blades". In: *Journal of Materials Processing Technology* 167 (2005), pp. 463–471.

[41] G.C. Larsen et al. *Modal Analysis of Wind Turbine Blades*. Risø–R–1181(EN). Roskilde, Denmark, 2002.

[42] J. L. Tangler and D. M. Somers. *NREL Airfoils Families for HAWTs*. NREL/TP-442-7109. Golden, Colorado, USA, 1995.

[43] Henrik Broen Pedersen and Ole Jesper Dahl Kristensen. *Applied Modal Analysis of Wind Turbine Blades*. Risø-R-1388(EN). Roskilde, Denmark, 2003.

[44] Dan M. Somers. *Design and Experimental Results for the S805 Airfoil*. NREL/SR-440-6917. Golden, Colorado, USA, 1997.

[45] W.A. Timmer and R.P.J.O.M. van Rooij. *Summary of the Delft University Wind Turbine Dedicated Airfoils*. AIAA-2003-0352. Delft, the Netherlands, 2003.

[46] J. Tangler and David J. Kocurek. *Wind Turbine Post-Stall Airfoil Performance Characteristics Guidelines for Blade-Element Momentum Methods*. NREL/CP-500-36900. Golden, Colorado, 2004.

[47] A. Baumgart. "A Mathematical Model for Wind Turbine Blades". In: *Journal of Sound and Vibrations* 251.1 (2002), pp. 1–12.

[48] P. Fuglsang and H. Madsen. "Optimization Method for Wind Turbine Rotors". In: *Journal of Wind Engineering and Industrial Aerodynamics* 80 (1999), pp. 191–206.